AD-A189 800 COUPLED HIGH POWER WAVEGUIDE LASER RESEARCH(U) UNITED 1/1
TECHNOLOGIES RESEARCH CENTER EAST HARTFORD CT
A J CANTOR ET AL 30 SEP 87 UTRC/R87-927184
UNCLASSIFIED AFOSR-TR-87-1747 F49620-85-C-0106 F/G 9/3 NL

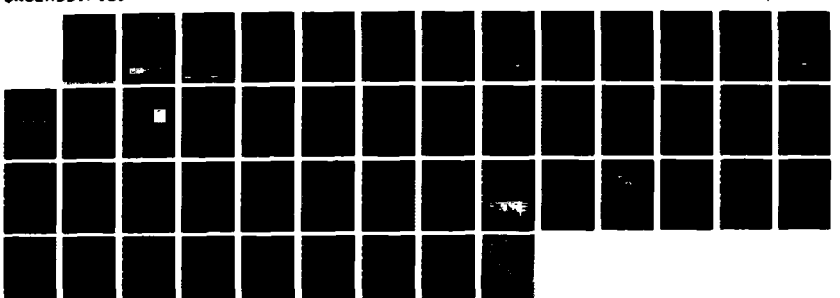

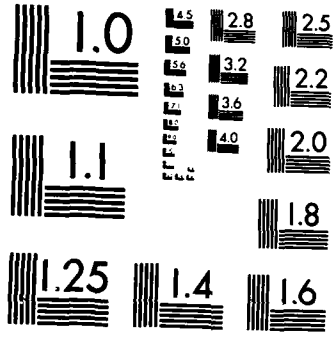

MICRCCOPY RESOLUTION TEST CHART
NATIONAL BUREAU OF STANDARDS-1963-A

R87-927184

(2)

AFOSR-TR- 87-1747

COUPLED HIGH POWER WAVEGUIDE LASER RESEARCH

Prepared by
A.J. Cantor
R.A. Hart
J.T. Kennedy
L.A. Newman

Final Report
September, 1987

Sponsored by the Department of the Air Force
Under Contract F49620-85-C-0106

UNITED TECHNOLOGIES RESEARCH CENTER
East Hartford, Connecticut 06108

Unclassified
SECURITY CLASSIFICATION OF THIS PAGE

REPORT DOCUMENTATION PAGE

1a. REPORT SECURITY CLASSIFICATION Unclassified	1b. RESTRICTIVE MARKINGS None
2a. SECURITY CLASSIFICATION AUTHORITY	3. DISTRIBUTION/AVAILABILITY OF REPORT Unlimited Distribution
2b. DECLASSIFICATION/DOWNGRADING SCHEDULE	
4. PERFORMING ORGANIZATION REPORT NUMBER(S) R87-927184	5. MONITORING ORGANIZATION REPORT NUMBER(S) AFOSR-TR- 87-1747
6a. NAME OF PERFORMING ORGANIZATION United Technologies Research Center 6b. OFFICE SYMBOL (If applicable)	7a. NAME OF MONITORING ORGANIZATION Same as 8a
6c. ADDRESS (City, State, and ZIP Code) United Technologies Research Center Silver Lane East Hartford, CT 06108	7b. ADDRESS (City, State, and ZIP Code) Same as 8c
8a. NAME OF FUNDING/SPONSORING ORGANIZATION Air Force Office of Scientific Research 8b. OFFICE SYMBOL (If applicable) NP	9. PROCUREMENT INSTRUMENT IDENTIFICATION NUMBER F49620-85-C-0106
8c. ADDRESS (City, State, and ZIP Code) USAF, AFSC Building 410 Bolling AFB, DC 20332	10. SOURCE OF FUNDING NUMBERS PROGRAM ELEMENT NO. 61102F; PROJECT NO. 2301; TASK NO. A1; WORK UNIT ACCESSION NO.

11. TITLE (Include Security Classification)
Coupled High Power Waveguide Laser Research (Unclassified)

12. PERSONAL AUTHOR(S)
A. J. Cantor, R. A. Hart, J. T. Kennedy, L. A. Newman

13a. TYPE OF REPORT	13b. TIME COVERED	14. DATE OF REPORT (Year, Month, Day)	15. PAGE COUNT
Final Report	FROM 7/1/86 TO 6/30/87	September 30, 1987	

16. SUPPLEMENTARY NOTATION

17. COSATI CODES			18. SUBJECT TERMS (Continue on reverse if necessary and identify by block number)
FIELD	GROUP	SUB-GROUP	waveguide, coupled, laser

19. ABSTRACT (Continue on reverse if necessary and identify by block number)

The experimental and theoretical progress that has been made in the coupled high power waveguide laser research program is reported. A problem has been encountered with the hollow-bore ridge waveguide laser array approach in which multimode operation occurs when the array is increased to above three elements. Alternative waveguide geometries were explored with the objective of achieving both phase locked operation and mode discrimination for an array size of 5 elements. Three new waveguide geometries were investigated. Of these new geometries, a modified hollow-bore ridge waveguide, utilizing a staggered ridge, has been used successfully to obtain single mode operation. This array, with a gain volume equivalent to six waveguide lasers, produced an output of 68 watts. The theoretical effort has resulted in the development of a theoretical method for calculating the modes and frequencies of two coupled rectangular waveguides separated by an infinitely thin partition with a gap in it.

(Continued)

20. DISTRIBUTION/AVAILABILITY OF ABSTRACT	21. ABSTRACT SECURITY CLASSIFICATION
☒ UNCLASSIFIED/UNLIMITED ☑ SAME AS RPT. ☐ DTIC USERS	Unclassified
22a. NAME OF RESPONSIBLE INDIVIDUAL [redacted] HOWARD R. SCHLOSSBERG	22b. TELEPHONE (Include Area Code) [redacted] (202) 767-4900 / 22c. OFFICE SYMBOL NP

DD FORM 1473, 84 MAR 83 APR edition may be used until exhausted. All other editions are obsolete.

SECURITY CLASSIFICATION OF THIS PAGE
Unclassified

R87-927184

Coupled High Power Waveguide Laser Research

TABLE OF CONTENTS

LIST OF FIGURES

LIST OF TABLES

Related Information

The preparation instructions defined by the Coupled High Power Waveguide Laser Research contract request information concerning publications, presentations and inventions that occurred during the course of the contract. This information is provided below.

List of Publications:

1) L. A. Newman, R. A. Hart, J. T. Kennedy, A. J. Cantor, A. J. DeMaria and W. B. Bridges, "High Power Coupled CO_2 Waveguide Laser Array", Appl. Phys. Lett., Vol. 48, p. 1701, 1986.

2) R. A. Hart, L. A. Newman, A. J. Cantor and J. T. Kennedy, "Staggered Hollow-Bore Waveguide Laser Array", Submitted to APL; to be published about October 1987.

List of Presentations:

1) L. A. Newman, "High Power Coupled CO_2 Waveguide Laser Array", Presented at the MIT Optical Sensing Series, April 2, 1986.

2) L. A. Newman, R. A. Hart, J. T. Kennedy, A. J. DeMaria and W. B. Bridges, "High-Power Coupled CO_2 Waveguide Laser Array", Paper WF1, presented at CLEO '86, June 11, 1986, San Francisco, CA.

3) R. A. Hart, L. A. Newman and J. T. Kennedy, "Staggered Hollow-Bore CO_2 Waveguide Laser Array", Submitted to CLEO '87.

List of Patent Disclosures:

1) R. A. Hart, L. A. Newman and J. T. Kennedy, "Overlapping Round-Guide Waveguide Laser Array", November 3, 1986.

2) R. A. Hart, L. A. Newman and J. T. Kennedy, "Staggered Array Waveguide Laser", October 21, 1986.

3) R. A. Hart, L. A. Newman, A. D. Heath and J. T. Kennedy, "Alternating Ridge Coupled Waveguide Laser", October 23, 1986.

List of Professional Personnel Associated with the Research:

Mr. Richard A. Hart
Dr. Arnold J. Cantor
Dr. Leon A. Newman

R87-927184

Coupled High Power Waveguide Laser Research

1.0 INTRODUCTION

Since June 1, 1984, United Technologies Research Center (UTRC), under sponsorship of the Air Force Office of Scientific Research Contract Nos. F49602-84-C-0062 and F49620-85-C-0106, has been conducting research to explore unique ridge waveguide techniques for phase locking coupled waveguide lasers. The motivation for investigating coupled waveguide laser arrays is to scale their output power by one to two orders of magnitude greater than the present state-of-the-art (i.e., scale to power levels of 100 W to 1 kW) while maintaining single frequency operation. To meet this goal, scaling the previous two and three element work to a great number of elements is required.

Described in Section 2.0 is the second program effort which focused its attention on meeting this goal. It was found that the simple scaling of the ridge geometries used in the first program arrays lead to a loss in mode control. Consequently, multiple frequencies were generated. Three new hollow-bore waveguide array geometries were conceived. All to a degree reduced the number of modes which would simultaneously lase. One however, the staggered hollow-bore array, is low loss for only a single super mode of the array. Consequently, single mode operation of an array with six channels was demonstrated.

1.1 Background

The objective of this program is to study, both from an experimental and theoretical perspective, coupled high power CO_2 waveguide lasers. This study is concerned with, but not limited to, hollow-bore ridge waveguide laser arrays. The ability to achieve phase-locked operation of two- and three-element hollow-bore ridge waveguide laser arrays was demonstrated and reported (Ref. 1) under a previous AFOSR contract (F49620-84-C-0062). In the present program, we are exploring the scalability of the hollow-bore ridge waveguide array concept to larger linear arrays. This is being accomplished by fabricating, operating and characterizing a variety of laser arrays and by conducting analyses to help interpret the observed operational characteristics and point the way to improvements in the performance of the laser arrays.

The concept of coupled hollow-bore ridge waveguides and the technique used to RF excite the CO_2 laser mixture within the waveguides has been discussed previously in Refs. 1 and 2, but is illustrated again in Figs. 1-1 and 1-2 for convenience. The waveguides are formed by grinding slots into an Al_2O_3 or BeO ceramic slab and then placing this slab between RF electrodes. Optical coupling between the guides is accomplished by shorting the partition between elements to form a gap of dimension "a", permitting radiation in a waveguide to leak into adjacent waveguides. The coupling between waveguides is controlled by adjusting both the gap dimension "a" and the separation "b" between waveguides. In addition, the waveguide dimensions have been found to

HOLLOW-BORE RIDGED WAVEGUIDE ARRAY

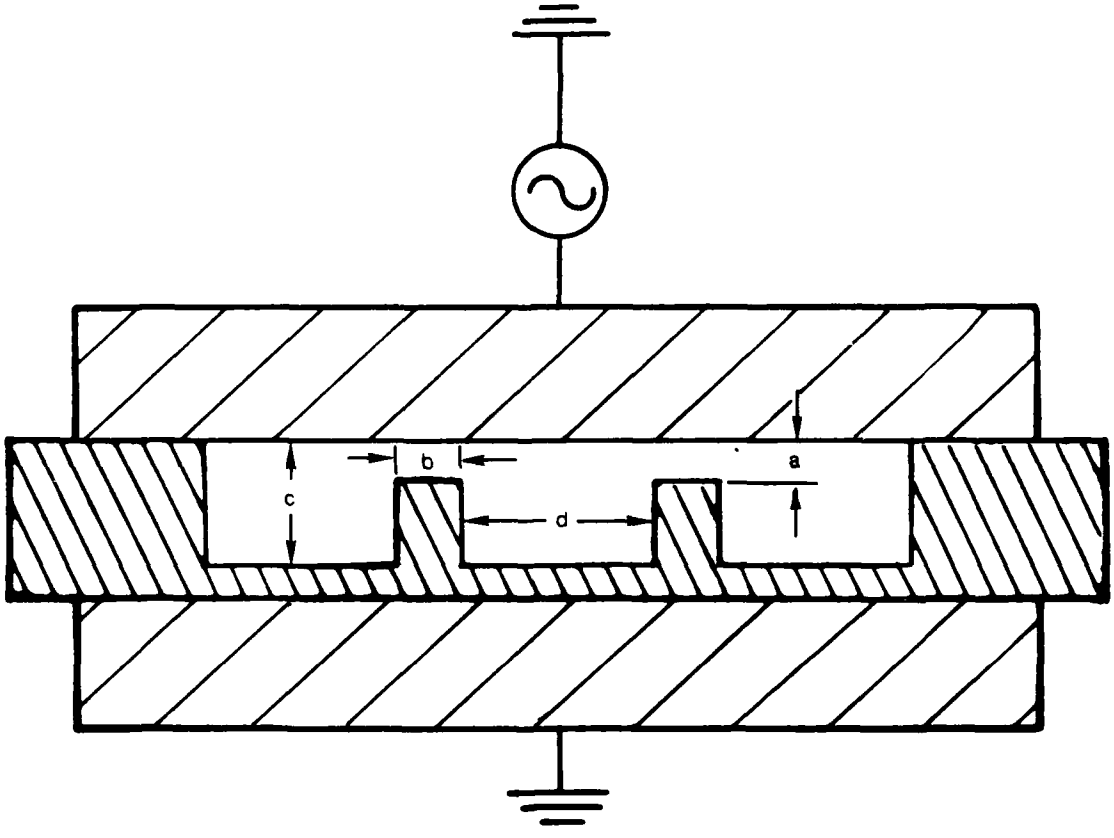

83-9-84-12

FIG. 1-2

UTRC RF EXCITATION CIRCUIT COMBINED WITH A WAVEGUIDE ARRAY

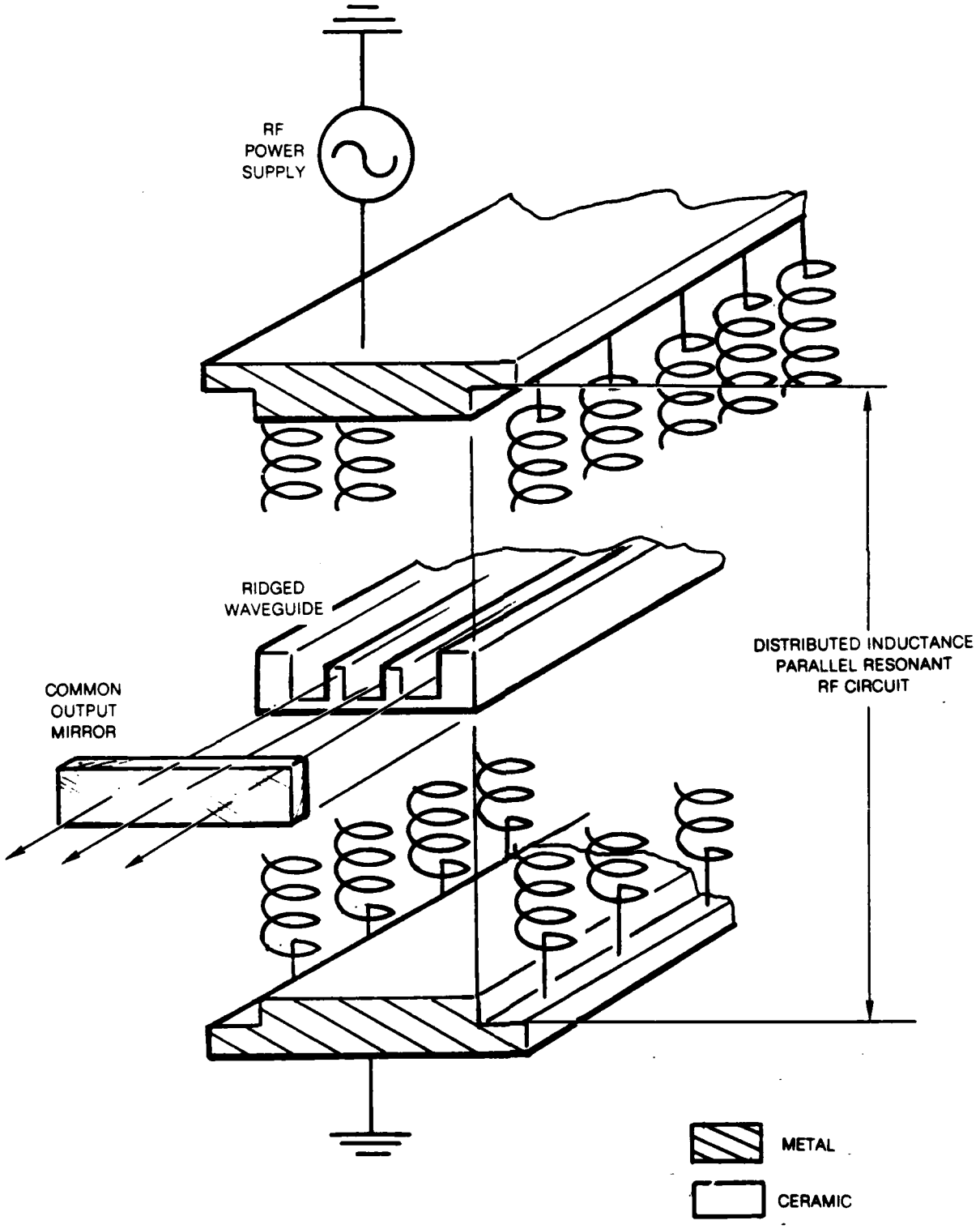

83-9-84-3

be important parameters in controlling both the amount of coupling between waveguide elements and the operating transverse mode.

Figure 1-2 illustrates the combination of the hollow-bore ridge waveguide concept with the UTRC developed RF-excitation circuit. The operation of the distributed inductance parallel resonant RF circuit is described fully in Refs. 3 and 4. The coupled waveguide resonator is formed by placing a flat common output mirror and a flat common total reflector within a few mm of each end of the waveguide.

As in the case of diode laser arrays, the motivation for exploring waveguide arrays of CO_2 lasers is to obtain output powers substantially higher than can presently be obtained from single channel or folded channel waveguide lasers while maintaining single frequency or near single frequency operation. This can be accomplished with an array because the problem of mirror damage is avoided by spreading the intracavity laser power over an area "n" times larger than a single element, where "n" is the number of elements in the array. A rule of thumb which appears to be well established is that single channel or folded channel waveguide lasers can be scaled up to the 100 W power level, whereas one can envision waveguide arrays which generate output levels from 100 W to multikilowatts.

This report describes the results that have been generated during the past two years. The experimental results are reported in Section 2.0. This section begins by describing the experimental setup and then is organized with the result obtained for the staggered array geometry. Section 2.0 concludes with near-field intensity scans for the staggered array in both coupled and uncoupled conditions. Section 3.0 describes the theoretical progress that has been made.

1.2 Program Summary

In general, steady progress has been made in improving the performance and basic understanding of high power coupled waveguide laser arrays. We have found that when the number of elements of the hollow-bore ridge waveguide array, as illustrated in Figs. 1-1 and 1-2, is increased to above three elements, a problem arises in which gap dimensions which are large enough to obtain sufficient optical coupling to achieve phase locking of channels, also results in multimode operation. Thus, the bulk of the experimental work conducted under this contract has been directed toward devising array geometries which yield both phase locked operation and mode discrimination. Below we list some of the more important results of the program.

1) The generation of over 100 W of output power from a partially phase locked, 5-element, 37 cm long waveguide array.

2) Determination of the minimum spread of beat frequencies of a non-coupled five-element array and the physics associated with establishing this minimum beat frequency spread (Ref. 5).

3) The invention of an alternating-ridge hollow-bore waveguide array structure which has been successful in suppressing multimode operation. Described in Ref. 6, Interim Report, "Coupled High Power Waveguide Laser Research," October 1986.

4) The invention of an overlapping round hollow-bore waveguide laser array which shows promise in yielding single frequency phase locked operation with improved efficiency relative to previous geometries (Ref. 5).

5) The invention of a staggered array of hollow-bore waveguide lasers which is the gas laser analog of the Y-junction diode array (Ref. 5).

6) Measurement of the gain profile within a four-element hollow-bore ridge waveguide revealing a highly nonuniform gain within each element and gain within the gap region (Ref. 5).

7) Development of a theoretical method for calculating the modes and frequencies of two coupled rectangular waveguides separated by an infinitely thin partition with a gap in it. Numerical results have been obtained for the gap centrally located in the partition as well as for the gap located to one side.

2.0 DESCRIPTION OF THE EXPERIMENTAL EFFORT

2.1 Experimental Setup

Figure 2-1 is a schematic illustration of the waveguide laser array test bed used for this program. It consists of four major components: a water cooled aluminum vacuum housing with an antireflection coated ZnSe window; a PZT actuated translating total reflecting mirror; a 37 cm waveguide array which is an integral part of the distributed inductance parallel discharge circuit; and a PZT actuated, tilting, partial reflecting, ZnSe output coupler. All the experiments conducted under this program used a 37 cm array length. By translating the total reflecting mirror, the cavity length of the array elements are tuned in unison, thus enabling tuning of the entire array to an operating frequency close to line center of the 10P20 rotational transition. By tilting the output coupler with a PZT actuator as illustrated in Fig. 2-1, a precisely controllable linear variation in the relative cavity length of the array elements can be made. This adjustment allows for compensation of undesirable and inevitable variations in the cavity length of the array elements caused by initial alignment error and thermal induced tilting of the cavity mirrors. However, this adjustment will not compensate for nonlinear variations in the relative cavity lengths of the array elements such as that which can occur with curved mirrors or nonuniform pumping and heat removal. A ZnSe antireflection coated window was used as a vacuum window instead of the partial reflector, as was done in previous work, to eliminate pressure induced optical distortion of the output coupler.

Figure 2-2 is a schematic of the experimental setup used to diagnose the operation of a waveguide array output. The output of the waveguide array was first directed through a beamsplitter located within a few centimeters of the array output. The reflected portion of the beam then propagated to an IR imaging screen to monitor the near field image of the array output. This diagnostic was use to determine if each element was operating on the same transverse waveguide mode. Furthermore, if phase locking between adjacent elements is achieved, interference fringes between elements occur and, therefore, provides a valuable diagnostic of the phase-locked condition of the array. Another portion of the beam is directed to a CO_2 rotational line analyzer to determine if all the array elements are operating on the same rotational line. Another sample of the beam is reflected off of a scannable beamsplitter onto either an infrared imaging plate or an apertured detector located in the far-field of the array. The image plate is used to provide a qualitative visual picture of the far-field mode pattern of the array, while the apertured detector is used to generate quantitative one-dimensional beam scans by scanning the beam with the scanning beamsplitter past the stationary apertured detector. Another portion of the beam is propagated through a focusing lens onto a high speed AuGe detector located at the transform plane of the lens. This detector is used to monitor mode beating and, therefore, is a valuable indicator of the mode purity of the array output. We have found

FIG. 2-1

37 cm WAVEGUIDE LASER ARRAY TESTBED

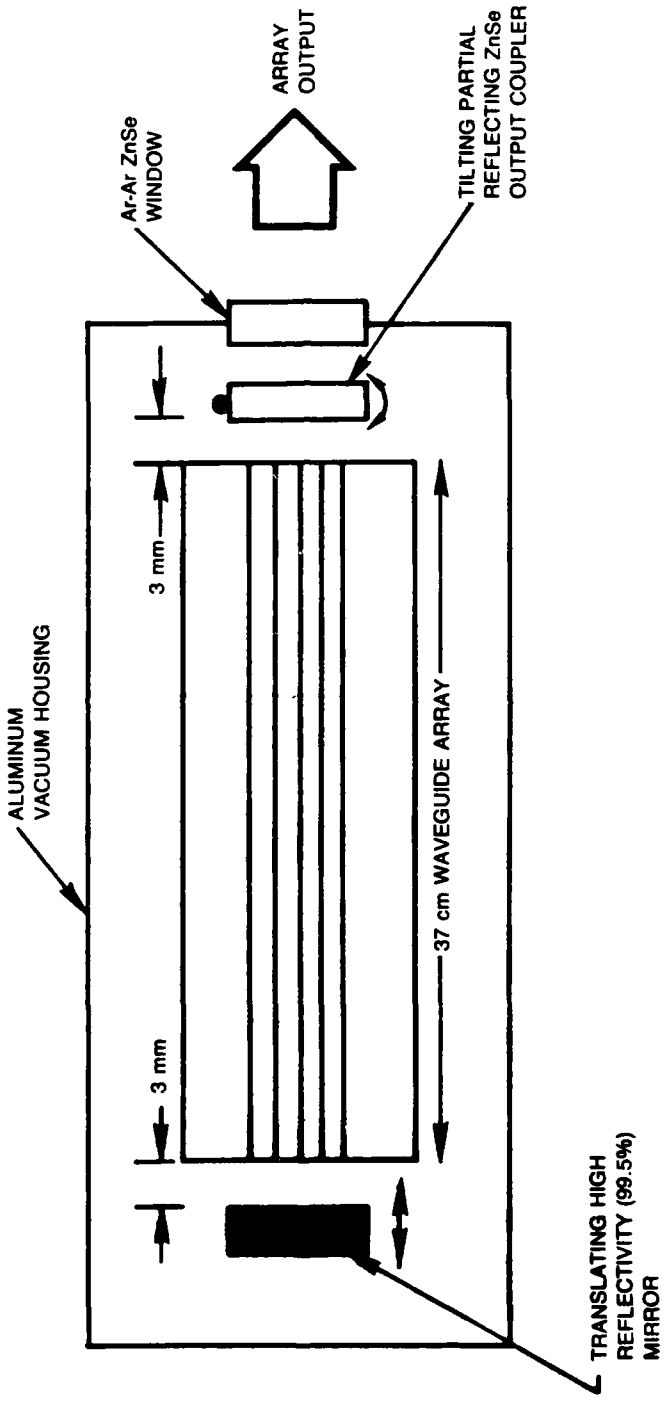

86-11-25-3

FIG. 2-2

DIAGNOSTIC CONFIGURATION FOR WAVEGUIDE LASER ARRAYS

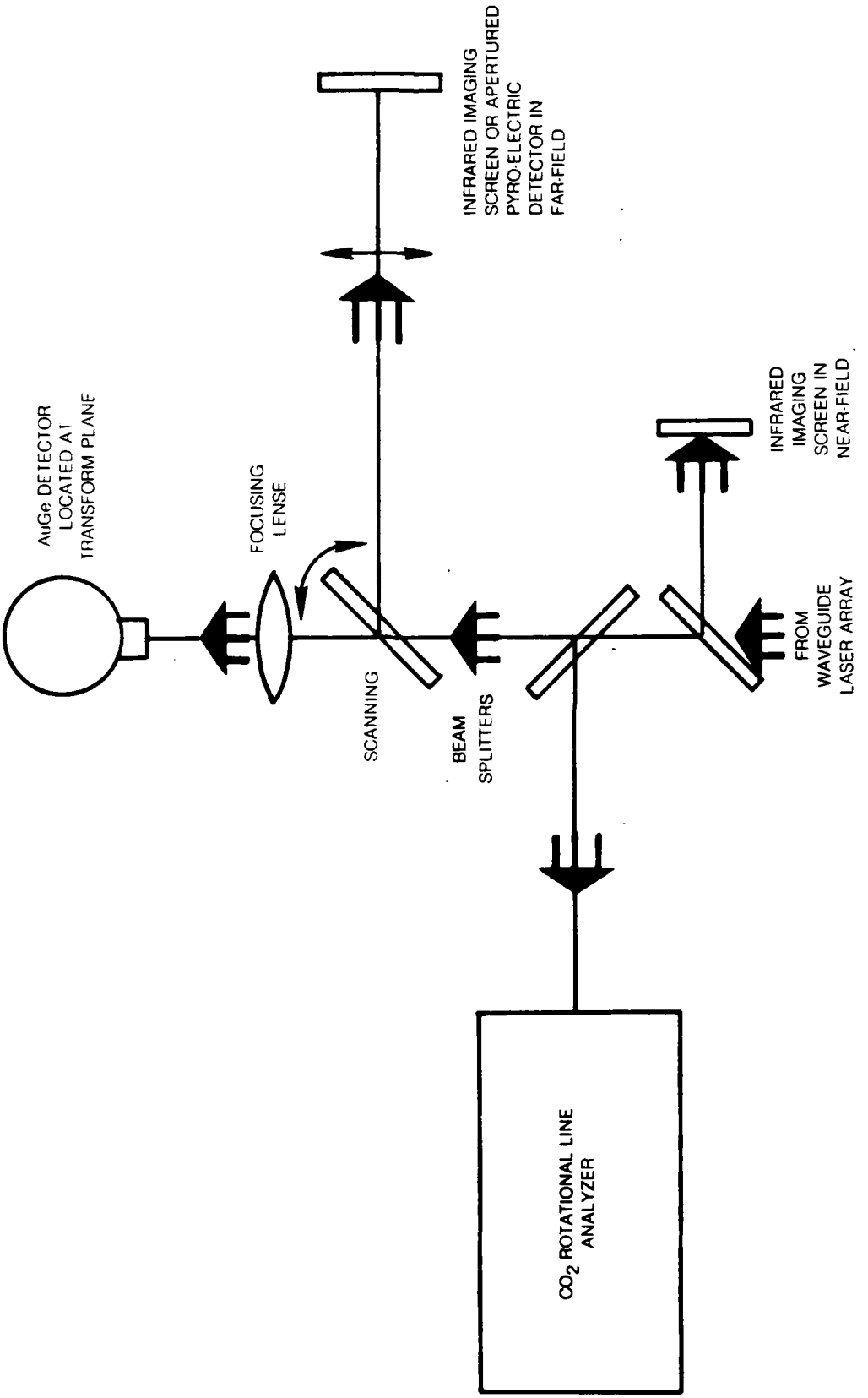

83-9-84-14

that the achievement of clean far-field fringe patterns does not always guarantee the achievement of single-frequency operation of an array.

2.2 Experimental Results for a Five-Element Hollow-Bore Ridge Waveguide Array

As documented in Refs. 1 and 2, single-frequency phase locking of two- and three-element hollow-bore ridge waveguide arrays has been demonstrated conclusively. In subsequent work, investigations were extended to five-element arrays.

From the perspective of power generation, excellent results were obtained. A maximum output power of 105 W was achieved from a five element array, which demonstrated that the output power increased with the number of elements at a rate of approximately 20 W per element. The waveguide geometry for this experiment consisted of five U-channel guides (Refs. 1 and 2), with a diameter of 2.25 mm, a separation of 0.25 mm, and a gape of 1.12 mm.

From the perspective of achieving phase locking, a number of problems were encountered. The near-field imaging of the array output revealed that when the inner three elements were operating on the lowest order EH_{11} waveguide mode, the outer two elements were operating on a higher order waveguide mode. The gain profile measurements revealed that the active medium residing in the outer waveguides is cooler than in the center three guides because of the additional cooling provided by the complete waveguide wall for the outer elements. Because the gas is cooler, it is optically denser which in turn results in a substantially different resonant frequency for the outer two waveguide elements relative to the inner three waveguide elements.

To help correct this problem, the ridge waveguide geometry illustrated in Fig. 2-3 was fabricated and tested. The difference between this waveguide geometry and that described previously is the addition of a thermal relief gap which inhibits the removal of heat from the outside walls, thus resulting in a more uniform gas temperature and more uniform resonant frequencies of the individual array elements. Indeed, after this modification was made, the near field pattern revealed that all the elements were operating in the EH_{11} mode. Furthermore, the far-field mode pattern consisted of two distinct lobes, suggesting that phase-locked operation of the array had been achieved. However, the high-speed detector revealed that there were a large number of mode beats, even though a fringe pattern was observed. The photograph in Fig. 2-3 is the mode beat spectrum of the array output which clearly shows that single-frequency operation of the array has not been achieved. A close inspection of the near-field image revealed that there was a considerable amount of power in the gap regions of the array. This observation leads us to the conclusion that the large open region created by removing wall material to form the coupling gaps also permits higher order mode oscillation in this region. This problem will get worse as the transverse dimension of the array

FIG. 2-3

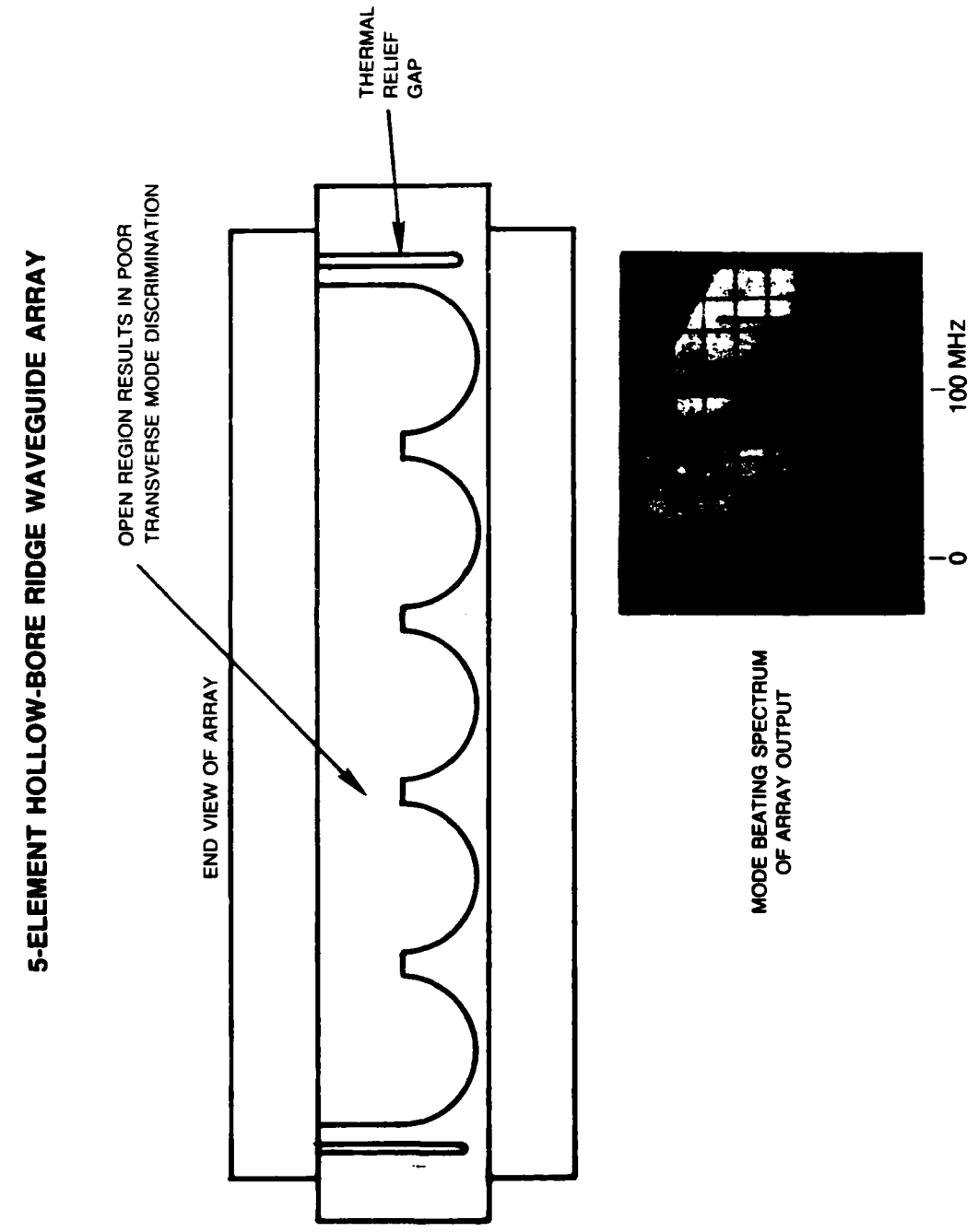

86-11-25-4

increases. In order to avoid this problem with the present geometry, one is driven to reduce the gap dimension, but this reduces the optical coupling and therefore, the locking range of the array. Thus, it appears that with the hollow-bore ridge waveguide geometry, we have a compromise situation between achieving adequate transverse mode discrimination and an adequate locking range. As the array size increases, it appears that it will become increasingly difficult to reach a satisfactory compromise with this hollow-bore ridged waveguide geometry

This fundamental compromise led us to the decision to explore alternative waveguide array geometries and associated array optical coupling techniques. The alternative techniques that have been explored are: 1) a coupled cavity array; 2) an alternating-ridge hollow-bore waveguide array; 3) an overlapping-round hollow-bore waveguide array; and 4) a staggered hollow-bore waveguide array. All of these array geometries, to a degree, reduce the number of modes lasing (Ref. 5), however, only the staggered array is capable of selecting a single supermode and discriminating against all others.

2.3 Staggered Hollow-Bore Waveguide Array

Recently, a new type of semiconductor laser array was demonstrated in which parallel single mode waveguides uncoupled along their lengths are coupled by Y-junctions in one region (Ref. 6). In order for radiation from the two limbs of the Y to couple into a nonradiating mode within the truck of the Y, it is necessary that the field within the limbs of the Y be in phase. Thus, by virtue of the junctions, the outputs of the waveguide arrays all radiate in phase to produce a single lobe in the far field. This accomplishment in the semiconductor lase arena motivated us to consider a hollow-bore waveguide geometry which could be considered the gas laser analogy of the Y-junction semiconductor laser array.

The staggered-array waveguide laser configuration and the techniques used to RF excite the CO_2 lasing gas mixture are illustrated in Fig. 2-4. The staggered-array structure was formed by first grinding 12 closely spaced parallel slots, each about 1 mm wide in the alumina slab. The thin partitioning walls separating these slots were then removed from alternate ends for a distance halfway down the length of the alumina waveguide slab, thereby forming the waveguides of 2.25 x 2.25 mm^2 in cross section for this portion of the structures, as illustrated in Fig. 2-4(b).

The lowest order mode which can propagate with low loss in one of the wideguide channels is illustrated in Fig. 2-4(c) and is the EH_{21}. The EH_{11} mode which would normally by the lovest loss mode in a conventional waveguide laser will be heavily attenuated by the dividing aperture walls. The EH_{21} mode, on the other hand, with its central on-axis intensity null, is not nearly as affected by the aperturing wall. Extending this low-loss mode

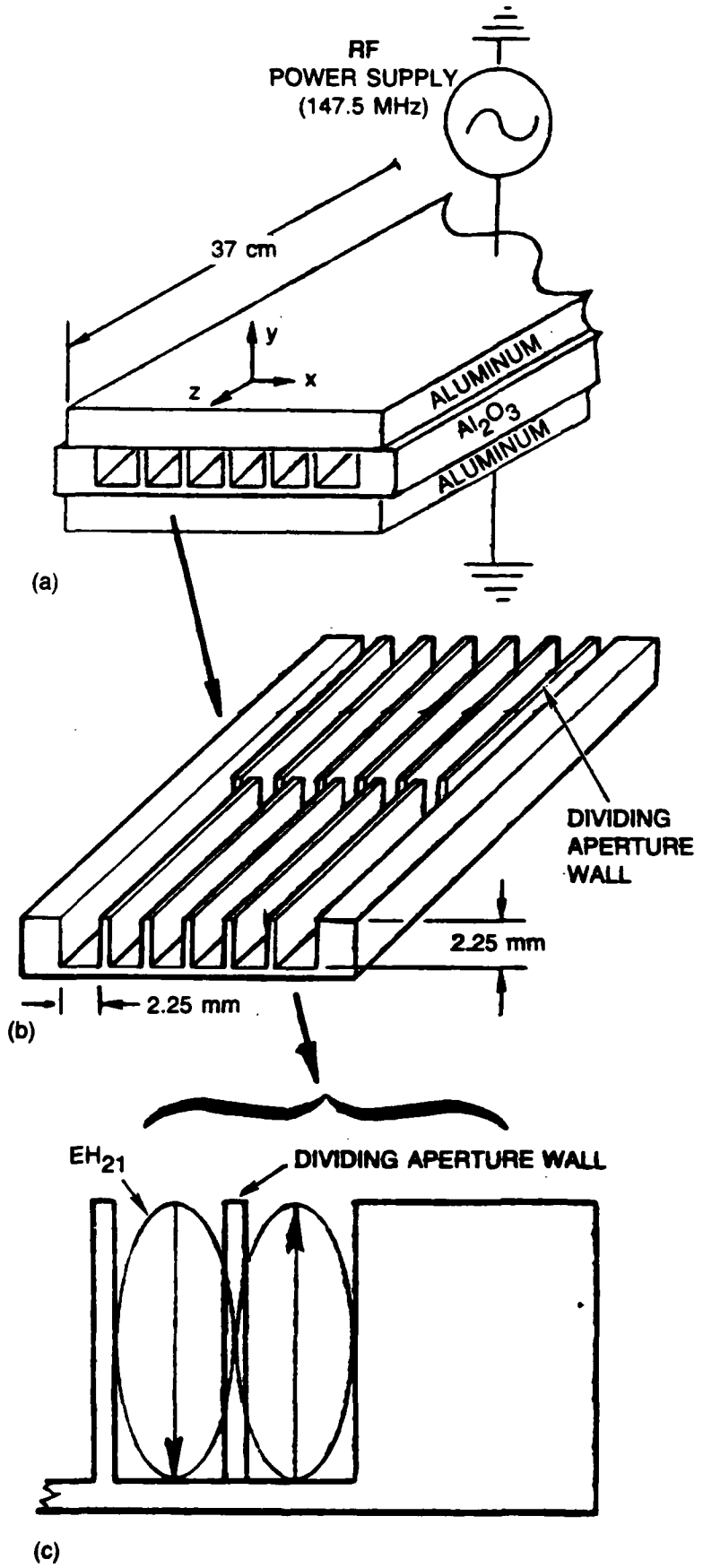

(a) Schematic representation of a six-element staggered array laser with RF excitation. (b) Staggered ridge hollow-bore alumina waveguide slab. (c) End view of one guide element. The dividing aperture wall begins at the halfway point along the length of the slab.

87-4-24-1

across the entire array width requires the array to be phase locked. If, for example, an adjacent pair of wall-divided E-field intensity lobes were not phase locked with a 180^{o} relative phase shift, they could not form the EH_{21} mode when propagating within the undivided region of the guide. As these independent intensity lobes propagate into the undivided region, they would each diffract. The field intensity would therefore increase within the central region of the undivided guide. This radiation, after reflection off an end resonator mirror, would propagate back to the dividing aperture all, where it would be attenuated by its front edge, as illustrated in Fig. 2-5. The staggered array, in effect, forms an intracavity spatial mode discriminator which has lowest loss for the antisymmetric supermode.

The staggered hollow-bore waveguide array illustrated in Fig. 2-4 was fabricated and tested. The groove width and depth were 0.040 in. and 0.090 in., respectively, and the wall thickness between waveguides was 0.010 in. Full phase-locking of the array was clearly achieved as revealed by the near-field pattern, the far-field pattern, and the high-speed detector. In particular, we note that robust single-frequency operation was achieved. The minimum detectable beat frequency for the array was 12 MHz. Only the antisymmetric mode was observed which is consistent with our expectations. Figure 2-6 is a far field intensity scan for the staggered array.

Although the staggered array demonstrated outstanding phase locking characteristics, the power performance of the array was poor. With 650 W of RF input, only 30 W of output was achieved. The poor performance is clearly due to the fact that the 0.101 wall thickness between waveguides which is 25 percent of the guide width results in very high intracavity loss. We have estimated the singe pass loss to be approximately 8 percent for the waveguide geometry used to generate the above results. Figure 2-7 shows the loss associated with a "thick" dividing aperture wall for the desired EH_{21} mode. Two additional arrays were fabricated in an effort to reduce this loss. The first had a reduced dividing aperture wall thickness of .127 mm and the second was fabricated in two halves so that a central opening was formed within the aperture wall as shown in Fig. 2-8. The table in Fig. 2-9 summarizes this data. It is clear that as the dividing aperture wall area is increased for a fixed guide element cross section, the higher the intracavity loss will be for the desired mode.

Further evidence of this problem exists in the near-field scans taken during the program. The intensity valleys corresponding to the position of the dividing aperture walls are clearly wider than those corresponding to undivided regions. Figure 2-10 is a near-field intensity scan for a rectangular-bore staggered array. Note that the width of the intensity valleys corresponding to the .254 mm aperture walls are wider than the others. The intensity valleys across the entire scans would have been equal width if there were no mismatch in the mode as it propagates from one end of the resonator to the other.

MODE DISCRIMINATION IN THE STAGGERED ARRAY,
LOCKED AND UNLOCKED CASES

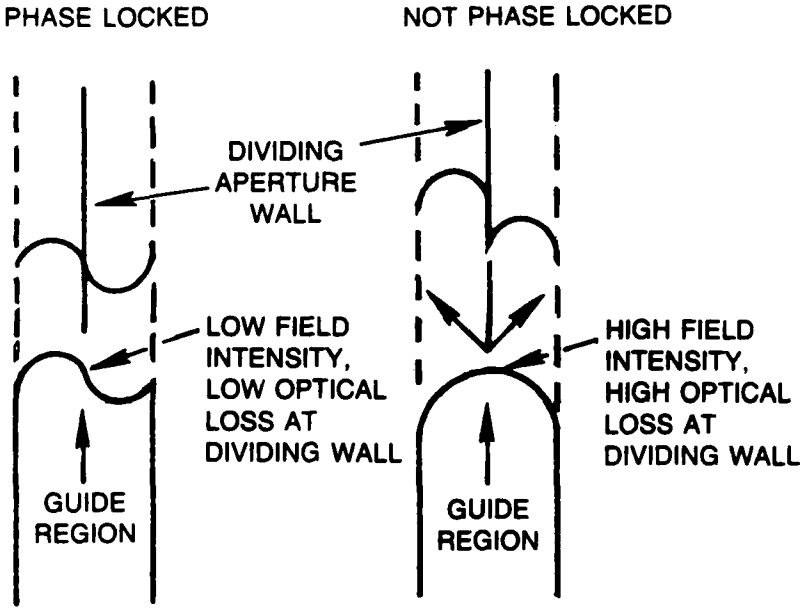

87-4-34-3

FIG. 2-6

FAR FIELD INTENSITY SCAN OBTAINED AT THE TRANSFORM PLANE OF A 1 METER FOCAL LENGTH MIRROR

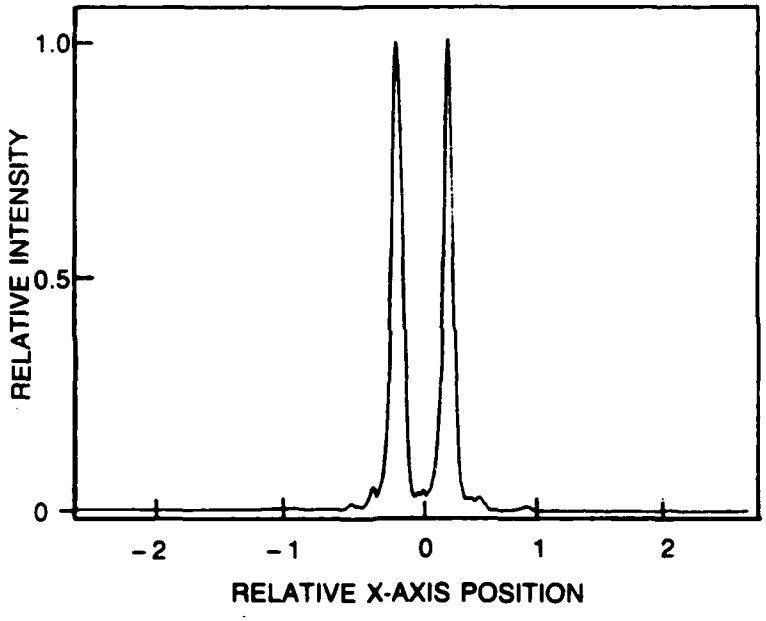

87-4-34-2

STAGGERED ARRAY MISMATCH FOR THE EH_{21} MODE

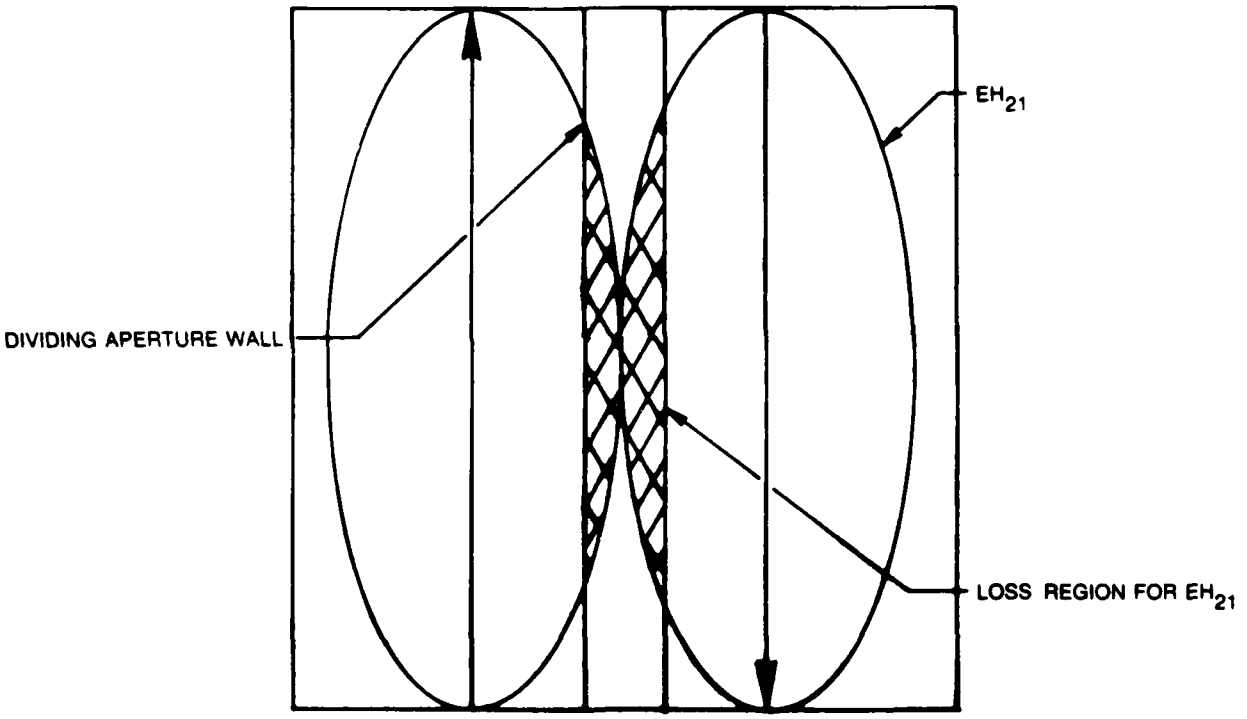

87-6-105-4

END VIEW STAGGERED ARRAY

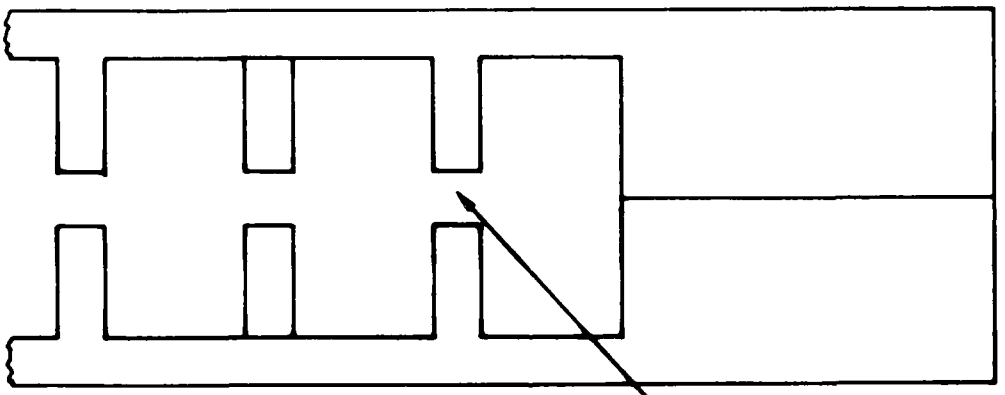

87-6-105-1

37 cm SIX CHANNEL STAGGERED ARRAY

ARRAY NO.	APERTURE WALL THICKNESS	LOCKING RANGE MHz	POWER OUT	EFFICIENCY
1	0.254 mm	12 MHz	30 Watts	4.6%
2	0.127 mm	17.5 MHz	40 Watts	7.2%
3	0.127 mm WITH 0.254 mm CENTRAL OPENING	13 MHz	68 Watts	5.4%

87-6-105-2

NEAR FIELD INTENSITY SCAN OF THE STAGGERED ARRAY

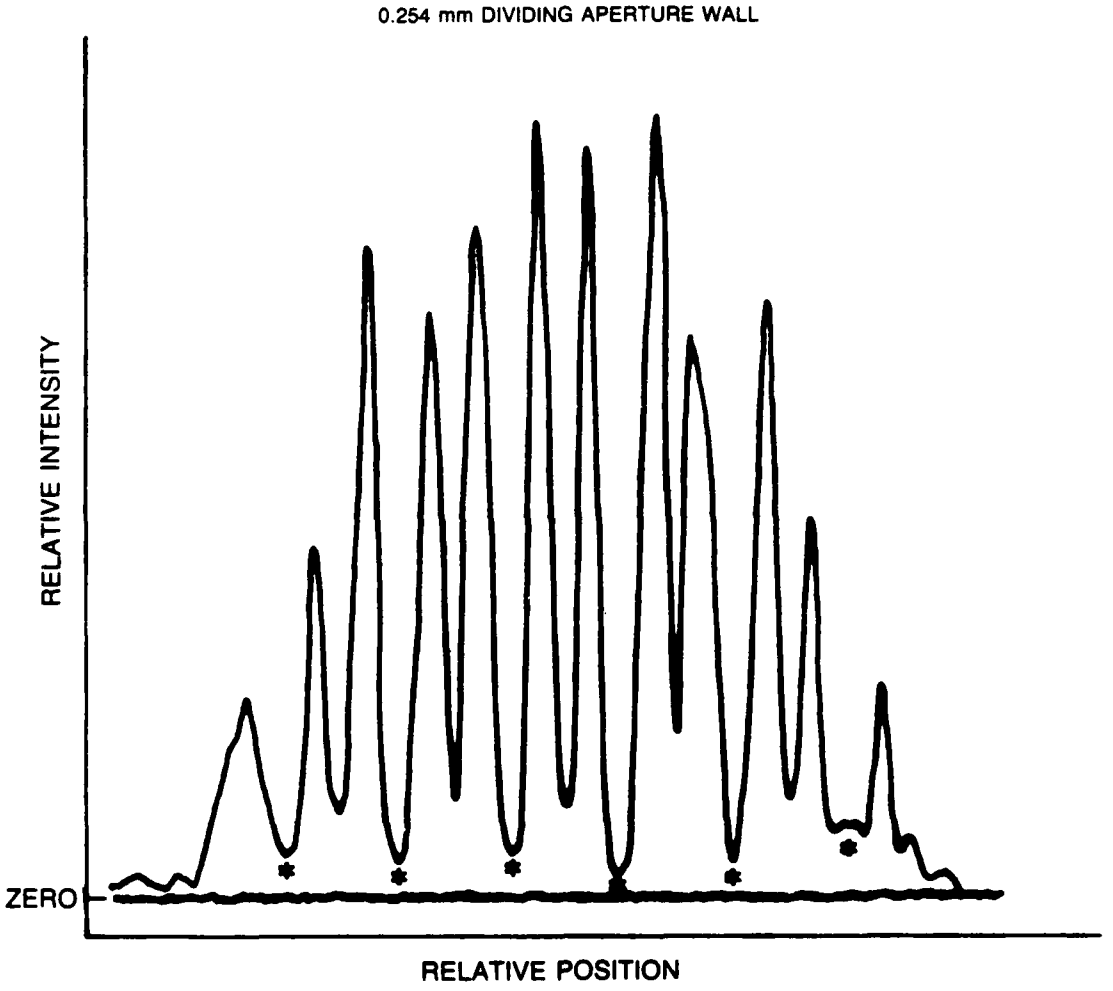

* INTENSITY NULLS CORRESPONDING TO THE POSITION OF THE 0.254 mm THICK DIVIDING APERTURE WALL

87-6-105-6

Figure 2-11 is a near-field intensity scan of a twelve element array which is not coupled. The near-field intensity profile of Fig. 2-11 is related to the phase locking of the array and not due to, for instance, uneven pumping of the array, as shown by the roughly even output of the uncoupled array in Fig. 2-11.

In conclusion, it is believed that by going to larger waveguide widths and smaller separations between walls, the intracavity loss of the staggered array geometry can be reduced substantially. For example, we estimate that if the wall width is increased from 0.040 in. to 0.090 in., and the separation between guides is reduced to 0.005 in., the intracavity loss decreases to 0.48 percent per pass which in turn will increase the output power and the efficiency of the array substantially. Thus, we have hope that the staggered hollow-bore waveguide array will yield simultaneous high power with good efficiency and single frequency operation.

NEAR FIELD INTENSITY SCAN OF TWELVE UNCOUPLED ELEMENTS

(1.0 mm WIDE x 2.25 mm DEEP)
0.127 mm DIVIDING WALL

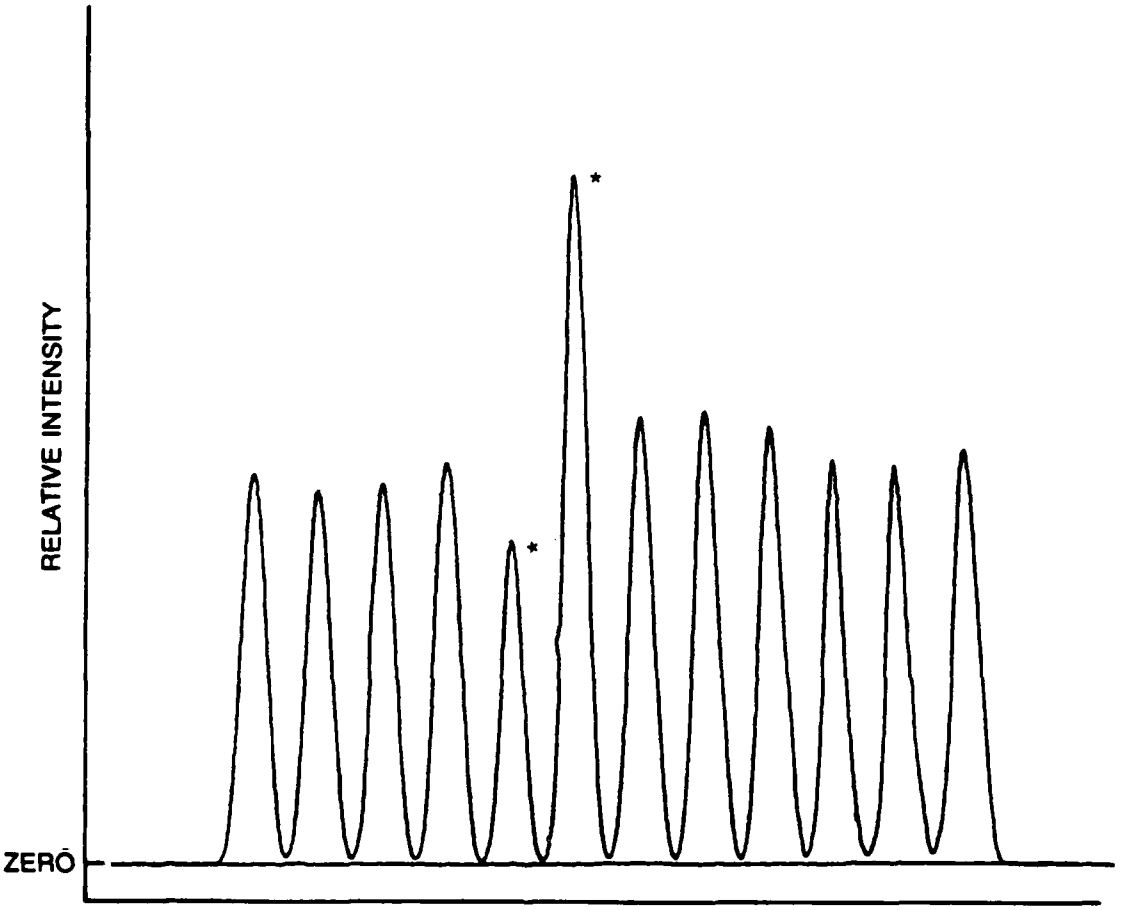

INTENSITY NULLS CORRESPOND TO
THE POSITION OF THE 0.127 mm
THICK DIVIDING WALLS

* ANONOUMOUSLY HIGH AND LOW INTENSITY PEAKS MAY BE DUE TO END DIFFRACTION COUPLING BETWEEN THESE TWO ELEMENTS AND SUBSEQUENT PHASE LOCKING

87-6-105-6 A

3.0 DESCRIPTION OF THE THEORETICAL EFFORT

3.1 Introduction

The overall goal of the theoretical effort is to achieve an understanding of the coupled waveguide lasers which have already been constructed and tested in Phases I and II sufficient (1) to provide guidance in the optimization of current designs, and (2) to begin to aid in the formulation of new and improved designs. A variety of tradeoffs are involved in the design of a waveguide laser array with high power and high efficiency, with a stable, single frequency, a useful supermode, and with robust phase-locking and a large locking range. But to study them systematically, reasonably accurate models of the arrays must be developed.

The following is a summary of progress in the analytical support and theoretical efforts in the first two phases of the program. The analytical support efforts are discussed first, with details presented in Sections 3.2 and 3.3. They consist of calculations of wall-attenuation losses and mode-mismatch losses. These are calculations that have been performed in support of the experimental program. The theoretical efforts are discussed next. They represent studies of fundamental aspects of coupled-wave-guide laser performance; waveguide modes and frequencies, supermode patterns, phase-locking, and thermal effects.

Examples of calculations of the usual per-unit-length propagation losses (i.e., wall losses) are presented, together with comments on their applicability to the staggered array, in Subsection 3.2. The extension to staggered-array geometries will be considered.

The staggered array geometry has, in addition to the usual wall-type losses that are measured per unit propagation length, a unique mismatch loss due to the discontinuity between waveguides with different guide cross-sections. The results of analytical calculations of the mismatch loss in simple rectangular geometries are presented in Subsection 3.3 as examples of the kinds of calculations which can be performed in support of the staggered array. Calculations for round and non-simple geometries will have to be done numerically.

Progress has been made in the analysis of the modes of coupled waveguides. The modeling of arrays has so far been confined to rectangular geometries and has ignored plasma and lasing effects altogether. Modeling has concentrated on understanding the supermodes and frequencies of coupled geometries, and the requirements for large locking ranges. The initial modeling in Phase I led to supermode relations for rectangular channels with infinitely thin partitions. In the first year of Phase II the thin-partition model was extended to the calculation of coupling constants. This model was not successful in explaining the beat frequencies and far-field intensities of

2- and 3-channel devices measured in Phase I. An effort was initiated to develop methods for calculating the modes of rectangular geometries with finite-thickness partitions. In the meantime, however, efficient computer programs suitable for waveguide analysis were developed independently at UTRC. Recent modeling initiatives undertaken in Phase II, based on these mathematical developments, have been more successful in explaining the Phase I data on beat frequencies. They also now permit the treatment of nonrectangular geometries, although no such geometries have yet been analyzed. The results of mode calculations are presented in Section 3.4 and of beat frequency comparisons in Section 3.5.

The new computer methods also provide the opportunity to find the correct supermodes for the geometries of interest, subject to the restriction that no lasing effects are included. It is now better understood that the supermodes for rectangular cavities with infinitely thin partitions can not be expected to adequately describe either rectangular cavities with finite-thickness partitions or round cavities. The former supermodes, derived in Phase I, are different, for example, from those first developed in 1984 to describe arrays of coupled semiconductor lasers (also referred to in the literature as diode or stripe arrays). The diode array supermodes have been shown to explain the far-field intensity data better than do the originally derived supermodes (see Sections 3.6 and 3.7). However, this alternative set of supermodes has not directly been shown to apply to the hollow-bore geometries, and is only presented as an example of the kinds of changes in supermodes that might emerge from improved calculations. The new numerical waveguide methods can be used to determine the supermodes.

The supermodes also depend on differences in resonant cavity frequencies among the channels. Such frequency differences can be caused by index-of-refraction differences arising from temperature differences, and need to be considered when comparing experimental data with theoretical models. Furthermore, lasing effects in connection with phase-locking can be expected to influence the distribution of laser powers in the individual channels, and need to be calculated. These issues are discussed in Section 3.8.

Thermal effects are an important feature in several aspects of the performance of waveguide laser arrays and need to be better understood. Several of these effects are discussed together in Subsection 3.9. Estimates of the effect of temperature differences on cavity resonant frequencies have been made, but have been of little use in understanding laser performance. Systematic studies of thermal effects remain to be carried out.

3.2 Wall Loss Calculations

Formulas for the attenuation coefficients for waveguide modes due to refraction into the walls are known for circular and rectangular cross-sectional channels. Methods exist for evaluating such coefficients for other

geometries (e.g., Ref. 7) but no use has yet been made of such methods in this program. In simple waveguides, the lowest-order mode also has the smallest attenuation coefficient.

Figure 3-1 is a graph of the intensity attenuation (or loss) coefficients for the four modes EH_{11}, EH_{21}, EH_{31} and EH_{41} for a rectangular channel of fixed height (90 mil, or 0.229 cm), and width varying from 90 mil (0.229 cm) to 180 mil (0.457 cm). The walls are of alumina, which in its single-crystal form, at any wavelength, has different dielectric constants depending on the orientation of the polarization. Values for 10.6 microns are taken from Ref. 8. The experiments make use of ceramic slabs composed of disordered polycrystalline alumina, so that an average of the single-crystal values is more appropriate. The average value used is $n = 0.64 + i0.037$.

The figure shows the expected $1/a^3$ fall-off with guide width, and the increase with mode number (m). Experimentally, 180-mil guides are subject to poorer mode control than 90-mil guides. This is believed to be due to the smaller differences between mode loss coefficients for the larger guides. The gains of these modes are comparable to one another, with some dependence on the gain profile across the channel. Hence, the loss plays a major role in determining which modes will lase and which will not, and in particular whether the lowest-order mode will have the highest net gain.

The figure can also be applied to the staggered array. The internal walls or partitions act to block or filter out the odd-m modes ($m = 1,3,...$) because these modes 'hit' a partition at their peak in the field profile. By contrast, the even-m modes ($m = 2,4,...$) hit a partition at a null. Thus, the $m = 1,3$ curves can be ignored, and the $m = 2,4$ curves used to estimate wall losses. Apart from the mode transformation that occurs at the discontinuity, the propagation in each uniform section of the guide is governed by Fig. 3-1.

These numbers, however, are expected to be only a lower-limit estimate of the true wall losses. In Ref. 9, a study of losses in a circular waveguide found that the losses in alumina were about a factor of 3 higher than predicted. These extra losses were attributed to either bends in the waveguide (i.e., departures from a true straight line propagation path), or to contaminant particles on the walls. Another possibility, which was not suggested in Ref. 9, is wall roughness. A simple argument can be shown to lead to the interesting result that a roughness contribution to the attenuation would also exhibit the $1/a^3$ behavior as does refractive leakage. It is interesting to note that the experimental curves in Ref. 9, though about three times higher than the ideal curves, do follow the same behavior with guide diameter. If the excess loss behaved differently (e.g., bend losses vary as a^3), the curves for total loss would show deviations from $1/a^3$. A separate experimental study would be required to separate out the contributions to loss in a satisfactory way. Some idea of the net loss, however, can be inferred from comparisons of lase data with a Rigrod laser analysis.

FIG. 3-1

MODE ATTENUATION — EH_{m1}

Al_2O_3 n = 0.64 – i0.037

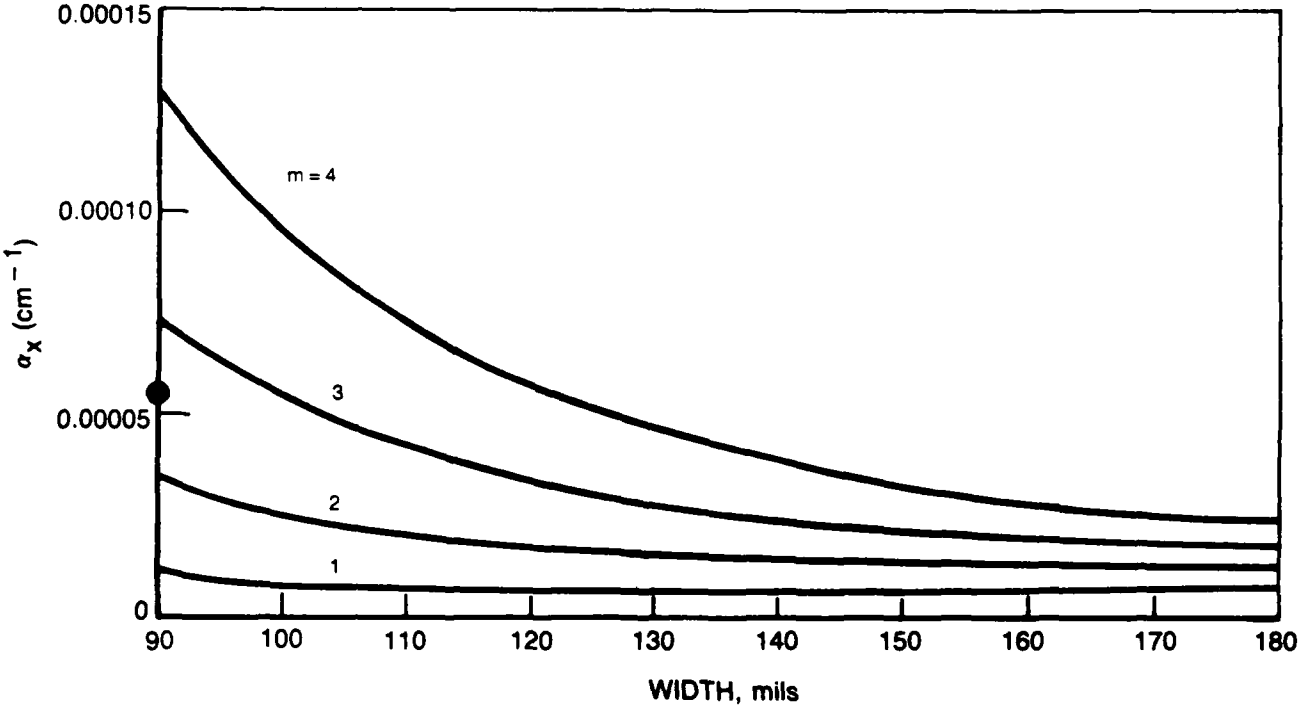

87-6-105-13

A direct measurement of loss in a 90 mil x 90 mil rectangular guide was carried out several years ago in another program. A lowest-order mode CO_2 laser beam containing a similar square channel was directly coupled into the channel in what was believed to be an optimum way. The result, a loss of 0.002 (0.2%) in a 37 cm length of guide, or 0.000054 per cm, is included (as a dot) on Fig. 3-1 for comparison with the m = 1 curve. The value is about four times the curve value of 0.000013. Some of the difference may be due to imperfect matching of the laser beam to the lowest-order guide mode.

3.3 Mode Mismatch Calculations

A waveguide is a channel whose cross-sectional shape and size is constant along its full propagation length. The staggered array consists of two different sections which are separate waveguides in this sense, and which are butted up to one another. Modes exist in each section, and energy propagating in one mode of the first section towards the second section will make a transition into the modes of the second section. If there is a mode in the second section which closely resembles the first mode, most of the incoming energy will transition to that mode, and the rest will be distributed among the remaining modes. Generally speaking, in a laser only one of the lowest-order modes, the one with lowest propagation loss in the waveguide, is able to lase, and all other modes are rejected because of their greater loss. For the lasers of interest, the propagation loss caused by the discontinuity in cavity shape is quite a bit larger than the single-pass loss due to wall effects. Thus, the transmission factor describing the percentage of power transferred from the laser mode in the first section to the laser mode in the second section is an important quantity to calculate.

The standard mathematical procedure for calculating the transmission factor in the case of a mismatch of the modes in the two sections is to evaluate the square of the overlap integral of the two normalized mode functions in their common aperture plane. This is an approximation which is valid when the total reflected power is small; i.e., when the transmission factor is close to unity.

In the simplest staggered array geometry, rectangular channels of width a, separated by walls of thickness 2t, are first ground out of the ceramic block, and then one-half of each wall is ground away from alternate ends of successive walls, leaving channels which are 2a + 2t wide running half the length of the guide and interrupted by a wall for the other half. There are also two end half-channels that are still of width a. In Fig. 3-2, one of the inner channels is illustrated with its neighbors, and the sine-shaped modes that fit into them. A typical transmission factor for the inner channel is calculated by finding the overlap integral between $x = -(a+t)$ and $x = +(a+t)$. The transmission factor is

MODE MISMATCH GEOMETRY — STAGGERED ARRAY

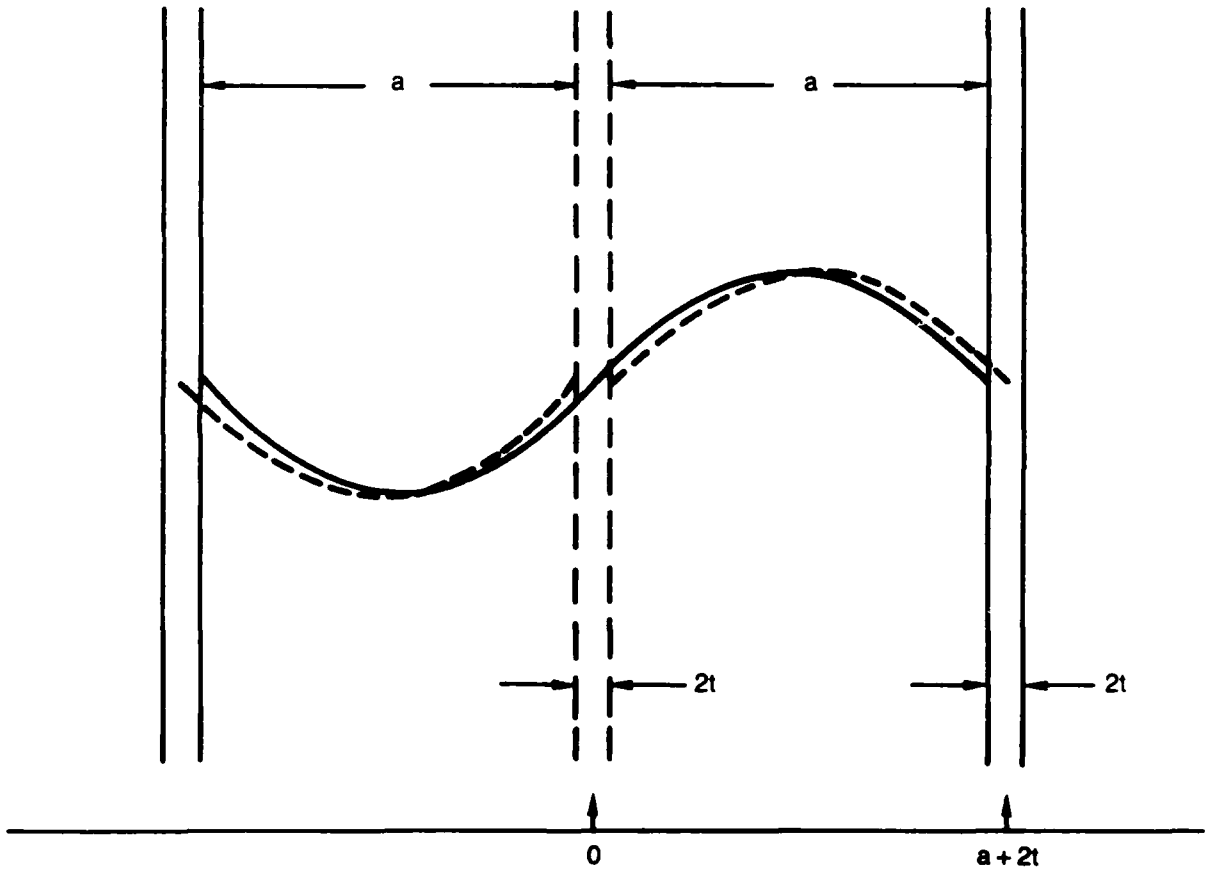

87-6-105-12

$$T_{12} = [(1 - u)\cos(\pi u) + (\pi^{-1}\sin(\pi u)]^2 \qquad (3\text{-}1)$$

where $u = t/(a + t)$. The "mismatch loss" may be identified with $1 - T_{12}$. As a numerical example, if $2a = 80$ mil (0.203 cm) and $2t = 10$ mil (0.0254 cm), then $u = 0.1111$, and the loss is .113, or 11.3 percent. By cutting the wall thickness down to $2t = 5$ mil (0.0137 cm), or $u = .0588$, the loss can be reduced to 0.033, or 3.3 percent.

The mismatch loss has also been calculated for the end channels. The transmission factor is

$$T_{12} = [4(1 - u)/\pi^2 u^2 (2 - u)^2]\sin^2(\pi u), \qquad (3\text{-}2)$$

For the same two cases treated in the previous paragraph, the calculated one-way mismatch losses are 4.3 percent (10 mil wall) and 1.2 percent (5 mil wall).

There is some indirect experimental data with which to evaluate the correctness of the above estimates. Lasing experiments were carried out, as reported elsewhere, on staggered arrays with rectangular channels with 10 mil and 5 mil walls. For these two cases, povers of 30 W and 40 W were measured. These numbers were introduced into Rigrod analyses from which rough estimates of the net propagation loss was obtained. These are 8 percent and 6 percent, respectively, which are "in the right ballpark" when compared with the calculations, but are not especially close.

3.4 Waveguide Laser Modes

The characteristic modes and frequencies of "empty" coupled waveguides (i.e., ignoring the effects of the lasing medium) were derived in Phase I (Ref. 10) and in the first year of Phase II (Ref. 11) from a simplified model: rectangular channels coupled by infinitely thin partitions with openings. Because the resulting modes have not proven adequate to describe any of the systems so far tested, we have used new numerical methods to calculate the modes and frequencies for geometries of practical interest.

The single-frequency eigenmodes of a dielectric waveguide are well-known for circular (Ref. 12) and rectangular (Ref. 13) channels, and approximate (but accurate) analytical formulas exist for them which given for each mode the electric and magnetic field components, the (longitudinal and transverse) propagation constants, and the attenuation (loss) coefficient (which is the imaginary part of the longitudinal propagation constant). When two or more

parallel channels are coupled by opening the walls between them, the resulting enlarged channel has its own modes for which, however, there are no analytical results comparable to those for single channels. Nonetheless, these multichannel modes can be studied by finding numerical solutions of Maxwell's equations. In fact, numerical solutions are required even for some of the single-channel geometries of interest. Computer methods for solving Maxwell's equations in arbitrary two-dimensional geometries (such as waveguides) have recently been developed at UTRC for semiconductor device modeling, radar cross-section modeling, and microwave waveguide analysis. The program developed for microwave waveguides has now been applied to the dielectric waveguide problem, by making use of a simplifying assumption to be discussed below, for two coupled rectangular channels with a finite rectangular partition between them.

The heart of the computer method is an efficient Helmholtz eigensolver (an algorithm to solve for the eigenvalues and eigenfunctions of the Helmholtz operator) based on an arbitrary triangular grid of mesh points. Mesh generation is based on the Delaunay triangulation method. The Helmholtz eigensolver uses finite-differences in an integral formulation referred to as the control region approximation, and implements local flux conservation through what is referred to as the flux-cell approximation. Eigenvalues are found by iteration using the method of Davies and Muilwyck, which is a variant of the power method. The computer program MCGUIDE developed for waveguides is presently suitable only for a homogeneous, simply-connected region with mixed, homogeneous boundary conditions.

In applying MCGUIDE to a two-channel system, an approximate boundary condition was used, namely, the vanishing of the dominant field components on all walls. This condition is suggested by the known approximate analytical solutions for a single rectangular or circular geometry. The electric fields in such a guide consist of large and small terms. The large fields vanish at the dielectric walls; they represent waves guided by the large reflection coefficient they see at grazing angles of incidence. The small fields represent the small amount of refraction into the walls occurring even at grazing angles. The dielectric waveguide is intrinsically 'leaky', but if the guide dimension is much larger than the wavelength, the amount of loss due to this leak is acceptably small for the lowest-order modes. For the purpose of calculating the fields and frequencies, it is sufficient to ignore the loss terms altogether.

Calculations were carried out for two 90 mil x 90 mil (0.229 cm x 0.229 cm) square channels separated by a 12 mil (0.0305 cm) partition with an opening that varied from 10 percent to 90 percent of the total height. Figure 3-3 shows the geometries for the 10 percent and 50 percent openings, together with the triangulated meshes in the two cases. Figure 3-4 presents calculated contour plots for the amplitude of either the horizontal (x-polarized) or the vertical (y-polarized) component of the electric field for the two lowest modes of the 10 percent-coupling guide. Figure 3-5 presents the analogous

FIG. 3-3

COUPLED SQUARE WAVEGUIDE CHANNELS WITH TRIANGULATION

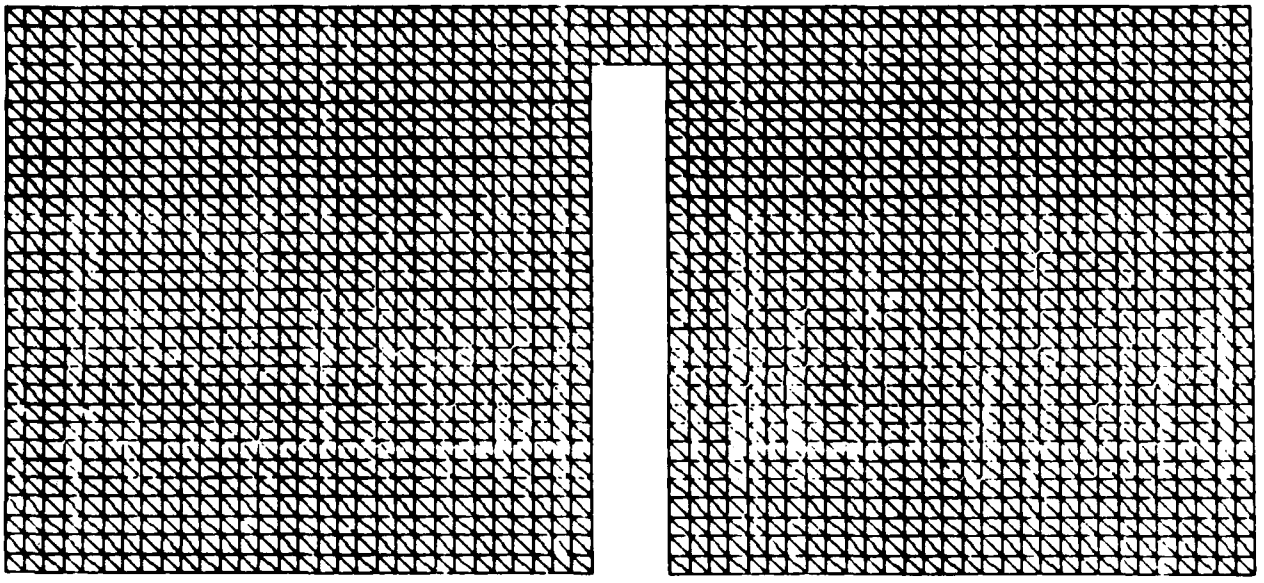

10% COUPLING

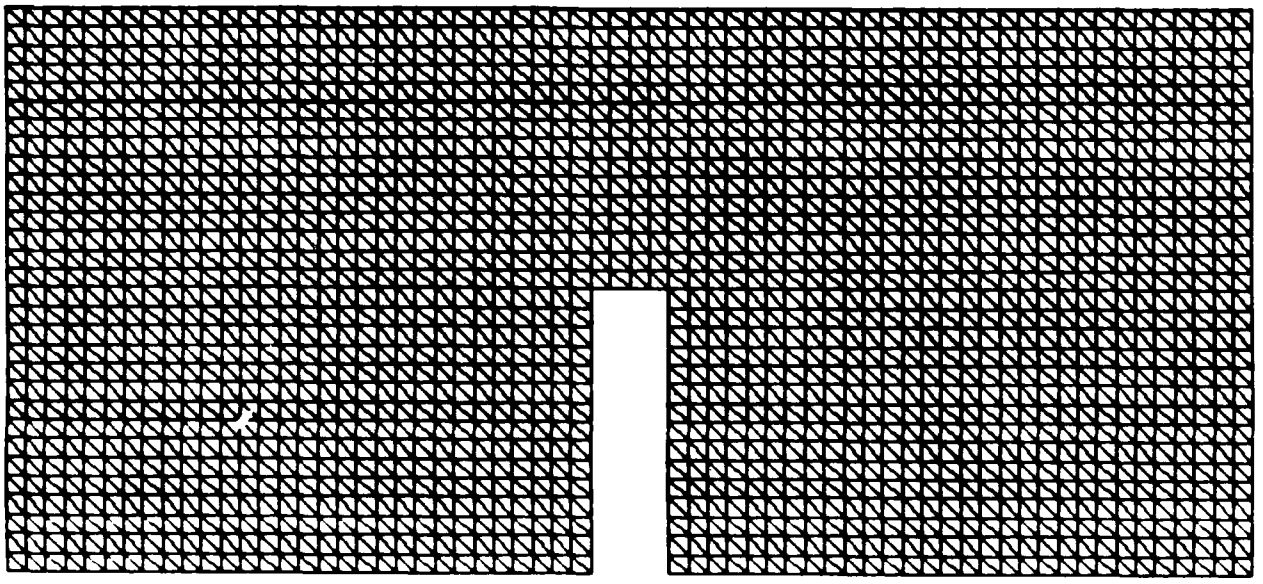

50% COUPLING

87-6-105-9

DOMINANT ELECTRIC FIELD CONTOURS

10% COUPLING

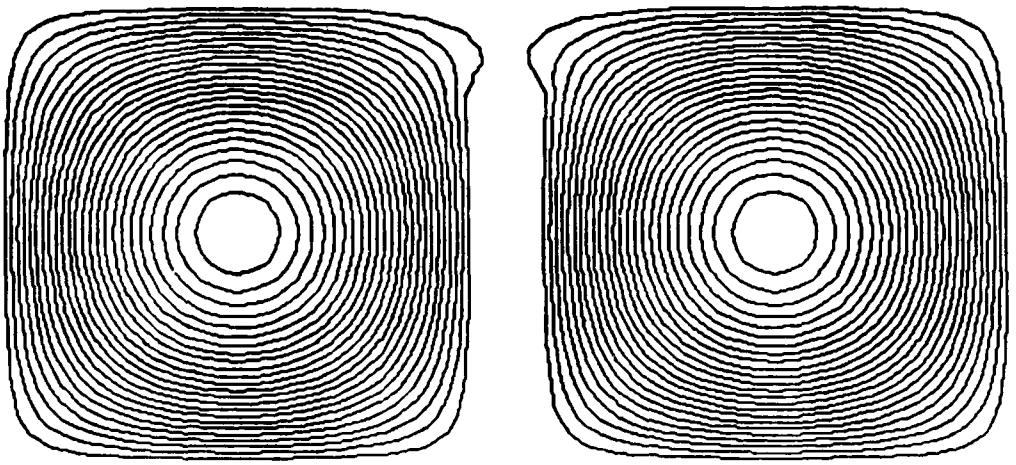

SYMMETRIC

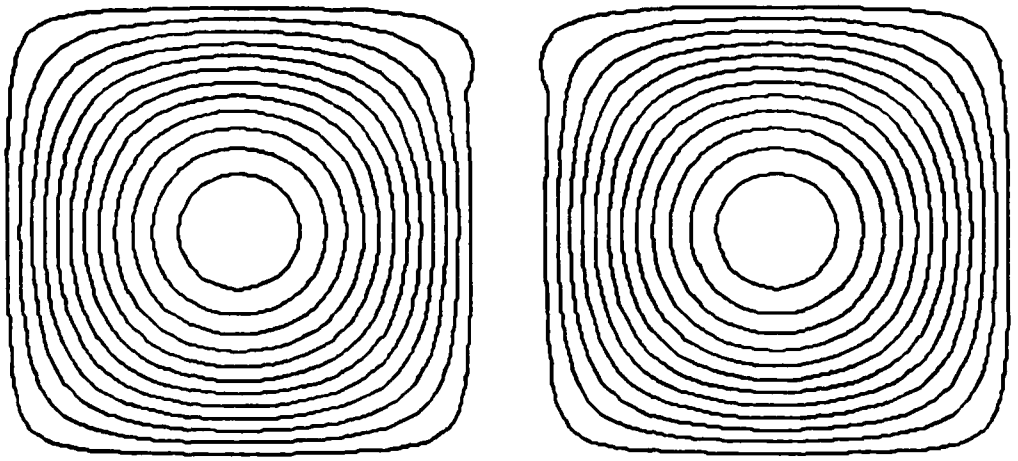

ANTI-SYMMETRIC

87-6-105-10

FIG. 3-5

DOMINANT ELECTRIC FIELD CONTOURS

50% COUPLING

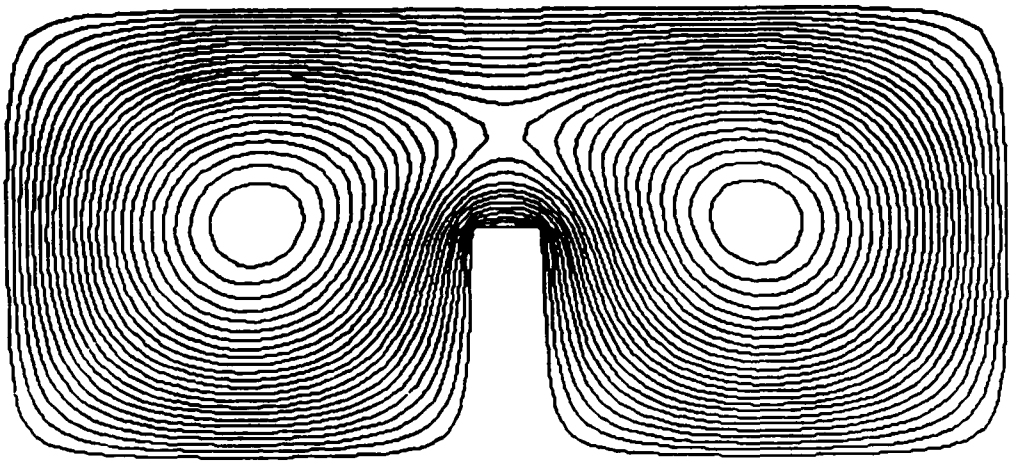

SYMMETRIC

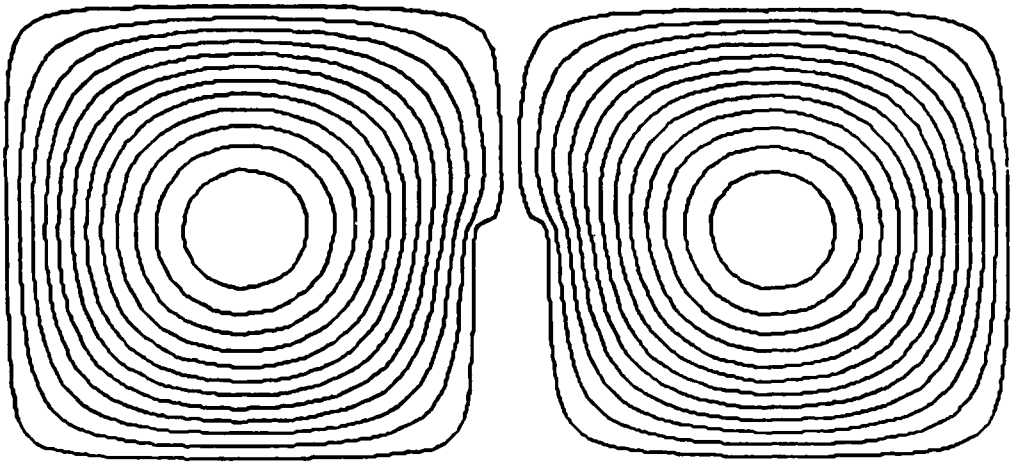

ANTI-SYMMETRIC

87-6-105-11

plots for a 50 percent coupling. The two lowest modes are known as symmetric (or even) and antisymmetric (or odd) modes because of the symmetry of the amplitudes with respect to the centerline separating the two channels. The symmetric mode has amplitudes which range from zero (at the walls) to a nominal value of +1 near the centers of both channels. The antisymmetric mode amplitudes are exactly zero on the centerline, and range from +1 near the center of one channels to -1 near the center of the other. The total range of amplitude values in each case is divided into 25 equal intervals, which is why the contour lines on the symmetric plots are more closely spaced than on the antisymmetric plots.

For the interpretation of beat frequencies, to be discussed below, it is not absolute frequencies but only differences between frequencies of possible modes of the same cavity that are relevant. Table 3-1 below presents the frequency differences between the antisymmetric and symmetric modes for the calculated geometries. The symmetric frequencies are lower than the antisymmetric. Test calculations on known geometries indicate that the calculated eigenvalues are accurate to about 1 part in 1000.

3.5 Comparison with Measured Beat Frequencies

The beat frequencies (or "beats") in the output of a laser are measured by directing the output beam onto a sufficiently fast detector. Beats only show up *before the system phase-locks.* The minimum observable beat frequency (MOBF) is found by varying the tilt of the 100 percent mirror, which has the effect of varying the difference between the cavity frequencies of the two channels. The theory of phase-locked lasers (Refs. 14, 15) leads to two important formulas: (1) the difference of frequencies of the coupled system before phase-locking is taken into account (Ref. 16):

$$\Delta\omega = \sqrt{(\Delta\Omega)^2 + (2M)^2} \tag{3-3}$$

and (2) a relation for the locking-range, or the critical value $\Delta\Omega = (\Delta\Omega)_L$, at which the transition from unlocked to locked behavior takes place:

$$(\Delta\Omega)_L \approx 2M \tag{3-4}$$

This approximate result was estimated in Phase I (Ref. 17) from results derived by W. J. Fader (Ref. 18). When the difference in cavity frequencies $(\Delta\Omega)$ exceeds the coupling frequency (2M) phase-locking will not occur. Hence, the MOBF is approximately given by the critical value of $\Delta\Omega$:

TABLE 3-1

CALCULATED FREQUENCY DIFFERENCE BETWEEN ODD AND EVEN MODES

Gap (%)	Frequency Difference (MHz)
0	0. (exact)
10	0.0
20	0.0
30	0.5
40	2.4
50	7.4
60	16.3
70	26.9
80	37.2
90	45.3
100	50.0 (exact)

$$(\Delta\omega)_L \approx 1.4 \times 2M \tag{3-5}$$

But, 2M is the difference $\Delta\omega = 2\pi\Delta f$ in frequency between the odd and even modes when the cavity resonant frequencies are equal ($\Delta\Omega = 0$). Therefore,

$$MOBF = 1.4\ \Delta f \tag{3-6}$$

(Note: Equations (3-3) through (3-5) are all written in terms of angular frequencies, which are 2π times the ordinary (cyclic) frequencies. But Eq. (3-6) is written in terms of ordinary frequencies.)

Only one MOBF experiment from Phase I was done with a pair of square channels, and the dimensions of the channels and the width of the wall between them are precisely those used in the calculations above. The height of the opening (the gap) was 30 mil (0.076 cm), i.e., a 33.3 percent gap. Interpolation from the calculated results given a difference frequency of 0.9 MHz, so that the predicted MOBF is approximately 1.2 MHz, which is in good agreement with the experimental result (Ref. 19) of 1.4 MHz.

Although no calculations have yet been done for U-shaped channels, it seems plausible that the low-order modes and frequencies of U-shaped (and to a lesser extent of Q-shaped) channels are close to those of square channels of the same transverse dimensions. In fact, the lowest-order frequencies of square and circular guides differ by 17 percent, the circular being higher, so that the difference between square and U-shaped frequencies is probably half of this, the U-shaped being higher. A data point exists for two U-shaped channels separated by a 10 mil (0.025 cm) partition with a 50 percent gap: 11.0 MHz (Ref. 19). The calculated result for square channels with a 12 mil (0.030 cm) partition and 50 percent gap is approximately 10.3 MHz, which is reasonable since the calculated value should be slightly smaller because of both the square geometry and the thicker partition. Further calculations with nonrectangular geometries are required to remove the uncertainties in this argument.

In Phase I the same kind of comparison was attempted with theoretical results based on an infinitely thin partition. There were, however, no experimental cases that could be confidently modeled this way, and so the agreement was not as good. The present agreement between theory and experiment suggests that an understanding of the modes and frequencies requires improved modeling of the actual geometries. In the next subsection we discuss another area in which better agreement appears to depend on improved modeling of the geometries. Further comments on beat frequencies appear in Subsection 3.6.

3.6 Supermodes

In Phase I, the supermodes of the multichannel coupled dielectric waveguide, neglecting laser effects (i.e., for empty, passive resonant cavities), were derived from a model with infinitely thin partitions between the channels by Fader (Ref. 20). These supermodes, which will be referred to collectively as the F solution, differ fundamentally from those which were first derived in the context of semiconductor research on coupled laser diode arrays by Butler, et al. (Ref. 21) and Kapon, et al. (Ref. 22), and which will be referred to as the BK solution. Table 3-2 presents a comparison of the two different sets of supermodes when the number of channels is N = 2 and N = 3. For N = 2, there is no basic difference between the F and BK modes; the two amplitudes are equal in magnitude, and their signs are either the same (equal phase, symmetric mode) or opposite (180° out of phase, antisymmetric mode). But for N = 3, the ratios of amplitudes in the channels are very different although the phase relationships are identical. In particular, for the in-phase mode in which all the signs are the same, the F solution predicts that the end-channel intensities are one-quarter of the mid-channel intensity, while the BK solution (if it were applicable) would predict one-half.

Experimentally, there is no evidence that the end-channel output beams are only one-quarter, nor even one-half, as intense as the mid-channel output beam. However, they are somewhat less intense, judging from near-field burn patterns in lucite, though a quantitative estimate has not been derived. But nonetheless, it is possible to conclude from such observations that the semiconductor supermode amplitude distribution (the BK solution) does appear to be more correct than the thin-partition amplitude distribution (the F solution) for N = 3. The inclusion of lasing effects in the theory may help to better explain the distribution of intensities. The possible effect of temperature variations on the output of the separate channels should be estimated, also, as part of a comparison of theory and experiment.

Stronger evidence for the need to modify the F solution comes from the staggered array experiments. The staggered array configuration automatically and robustly favors the alternating-phase supermode. The F solution predicts that the amplitudes of all channels are equal. The BK solution predicts that the amplitudes are highest in the middle of the array and decrease in magitude in going towards either end. For N = 12, for which there is recent experimental near-field data, the BK solution predicts that the end channels have approximately one-quarter the amplitude, or one-sixteenth the intensity of one of the middle channels. The near-field intensity data (Fig. 3-3) shows a definitely nonuniform distribution of intensities, with the end channels having roughly one-quarter the average intensity of the middle channels. There appear to be individual differences between channels, but the overall appearance of the scan clearly favors a departure from the F solution.

The patterns of beat frequencies are also different for the two solutions. From the (angular) frequencies given in Table 3-2, one can form

TABLE 3-2

FREQUENCIES AND AMPLITUDES OF SUPERMODES

	Fader (UTRC)			Butler/Kapon		
N = 2	m = 1	2		m = 1	2	
$\omega^{(m)}$	- 2M			- 3M	- M	
$E_1^{(m)}$	2/2	1		3/2	3/2	
$E_2^{(m)}$	2/2	-1		3/2	- 3/2	
N = 3	m = 1	2	3	m = 1	2	3
$\omega^{(m)}$	- 3M	- M		- 2M - 2M	- 2M	- 2M + 2M
$E_1^{(m)}$	1/2	3/2	1	2/2	1	2/2
$E_2^{(m)}$	1	0	-1	1	0	-1
$E_3^{(m)}$	1/2	- 3/2	1	2/2	-1	2/2

one beat for N = 2, and three beats for N = 3. But whereas the single beat for N = 2 is the same (2M) for both the F and BK solutions, the sets of three beats are different. For the F solution, the beats form an arithmetic progression (M, 2M, 3M). (One ignores the sign of the difference in tabulating beats.) For the BK solution, two of the beats are identical (M', M', 2M', where M' = 2 M). Although the measured beat patterns should, in principle, contain evidence for or against these solutions, in practice it is very difficult to draw any conclusions. These patterns would show up most clearly when all the resonant cavity frequencies are the same, but in that case phase-locking eliminates the beats altogether. Independent measurements of the resonant frequencies would have to be made so that beats existing before phase-locking occurs could be analyzed.

The new computer methods reported above make it possible to calculate the empty-cavity supermodes for N = 3 and higher exactly as was done for N = 2. The result of such calculations would be the electric field distributions of the supermodes, their modal frequencies, and the pattern of amplitudes for each one.

3.7 On-Axis Intensity Ratios

The supermode amplitudes enter into the calculation of the far-field diffraction intensity pattern. In Phase I an attempt was made to compare measured and calculated on-axis intensities (i.e., measured at zero angle with respect to the direction normal to the array) for the in-phase supermode (also referred to as the 'symmetric' mode). The quantity calculated was the ratio of the on-axis intensity for that mode (which appears when the laser is suitably phase-locked) to the on-axis intensity when the laser is not phase-locked. These two conditions, called 'coherent' and 'incoherent', respectively, are easily recognized experimentally by a sharply defined multiple narrow-lobe pattern with its maximum intensity directly on axis (coherent, symmetric) and a single rounded lobe with no sidelobe detail (incoherent). The experimental patterns produced on thermally sensitive paper are shown in Fig. 8 of Ref. 10. The corresponding measured intensity profiles are shown in Fig. 9 of Ref. 10.

The diffraction pattern, and in particular the angular dependence of the far-field intensity on the angle in a direction parallel to the linear array, is the product of three factors: an element factor and obliquity factor, both which are the same for all supermodes, and an array factor which distinguishes the supermodes. On axis, the array factor is simply the square of the sum of the squares of the amplitudes, but the amplitudes are different from what they would be if the lasers were phase-locked. Pending a more complete analysis of phase-locking and supermodes, the following assumptions had to be made to proceed. Assumption (1): for the incoherent (non-phase-locked) case, the magnitude of each laser amplitude is equal to the same constant, which is taken to be 1 for simplicity. Thus, the on-axis array factor for the incoher-

ent case is 3. Now, if three equal-amplitude lasers could be locked together with equal phase, the array factor for the coherent case would be 9. This special case will be included in the comparison. Assumption (2): for the coherent (phase-locked) case, the amplitudes have the same ratios as are calculated for empty cavities, and the largest amplitude (which for N = 3 is the middle amplitude in the symmetric mode) is equal to 1. In other words, the middle laser is assumed to have as much laser power as an unlocked laser would have. The other lasers (the end-lasers) have lower power because the frequency pulling which accompanies coupling causes them to lase off line-center. Measurements on the 12-channel device show a non-constant set of amplitudes in the locked case. Measurements were not made to determine if the middle lasers have unit or near unit amplitudes, but this seems plausible.

Subject to the above assumptions, the comparison is outlined in Table 3-3. The N = 2 case is also included, and also the equal-amplitude N = 3 case. It will be seen that the BK symmetric supermode gives the better agreement with data. It needs to be pointed out, though, that the measurement range was not in the far-field as required. However, it seems reasonable to conclude that improved calculations of the supermodes, based on the use of the correct geometries and the inclusion of lasing and phase-locking effects, should be carried out because of the potentially valuable insights into array performance which such calculational capability can provide. Improved measurements of far-field profiles will be required also.

3.8 Phase-Locking and Locking Range

It can be seen from the above discussions that an understanding of the details of laser phase-locking is required to answer three key questions about the modeling of coupled waveguide lasers:

(A) How does phase-locking alter the empty-cavity waveguide supermodes and frequencies?

(B) How are the phase-locked intensities related to the non-phase-locked ones?

(C) Over what range of unequal cavity resonant frequencies will the phase-locked state be stable?

Development was begun in Phase II of a computer program, based on the approach of Spencer and Lamb (Refs. 14, 15), to answer these questions for N = 3 and higher. A similar approach was taken (Ref. 18) to the N = 2 case already referred to in Subsection 3-5 in connection with the comparison of measured and calculated beat frequencies. This approach does not model the actual coupling geometry simultaneously with the lasing. In fact, the laser medium is a highly idealized uniform gain medium. The coupling constants are determined ahead of time from empty-cavity calculations and introduced through

TABLE 3-3

FAR-FIELD ON-AXIS INTENSITY RATIOS

IR = I [Coherent (Symmetric)]/I [Incoherent]

	Theory	Experiment	
		Range = 2.0 m	5.8 m
N = 2 (Rayleigh Range = 3.0 m)			
(A) Equal Amplitude			
$I\ (Inc) = (1)^2 + (1)^2 = 2$	2	1.7	2.2
$I\ (Coh) = (1 + 1)^2 = 4$			
N = 3 (Rayleigh Range = 6.7 m)			
(A) Equal Amplitude			
$I\ (Inc) = (1)^2 + (1)^2 + (1)^2 = 3$	3	1.8	-
$I\ (Coh) = (1 + 1 + 1)^2 = 9$			
(B) Fader (UTRC)			
$I\ (Inc) = (1)^2 + (1)^2 + (1)^2 = 3$	1.33		
$I\ (Coh) = (1/2 + 1 + 1/2)^2 = 4$			
(C) Butler/Kapon			
$I\ (Inc) = (1)^2 + (1)^2 + (1)^2 = 3$	1.94		
$I\ (Coh) = (2/2 + 1 + 2/2)^2 = 5.828$			

effective coupling constants. It is believed that the answers to the above questions will apply to simple coupling geometries and may be applicable to the staggered array.

3.9 Thermal Effects

It is necessary to systematically examine thermal effects in coupled waveguide arrays, and in particular in staggered waveguide arrays, and to attempt to include such effects in the detailed models.

Thermal effects in coupled hollow-bore lasers depend on geometry because the walls are used for heat extraction as well as waveguiding. Temperatures in the plasma depend on the thickness and shape of the walls surrounding the channels. In a planar array, the variation in temperature from a channel in the middle of the array to one at the end of the array can be significant for mode control, phase-locking, and laser gain (Ref. 11). Experimental studies have been reported of a method for equalizing temperatures using thermal relief slots cut into the ceramic slab on either end of the array. Thermal analysis of a laser with and without the slots was carried out at UTRC in support of this idea.

Locking-range is related to geometry through temperature. The cavity resonant frequencies of the individual channels depend on temperature through the index of refraction of the gas mixture. Phase-locking is made more difficult by a spread of resonant frequencies among the lasers to be locked.

Furthermore, the temperature distribution in the plasma within a channel, and hence its gain profile, influences the preferred lasing mode, while the presence of gain or loss in the gaps between the channels influences the preferred supermode. Gain profiles were measured and reported (Ref. 11); calculations of the above gain in different modes and supermodes are possible with this data but have not yet been carried out.

REFERENCES

Sections 1.0 and 2.0

1. Newman, L. A., A. J. Cantor, W. J. Fader, R. A. Hart, J. T. Kennedy and A. J. DeMaria: Coupled High Power Waveguide Laser Research. Final Technical Report under Contract No. F49620-84-C-0062, July 30, 1985.

2. Newman, L. A., R. A. Hart, J. T. Kennedy, A. J. Cantor, A. J. DeMaria and W. B. Bridges: High Power Coupled CO_2 Waveguide Laser Array. APL, Vol. 48, No. 25, P. 1701, June 23, 1986.

3. U. S. Patent No. 4,443,877, Uniformly Excited RF Waveguide Laser, April 17, 1984.

4. U. S. Patent No. 4,363,126, Tuned-Circuit RF-Excited laser, December 7, 1982.

5. Cantor, A. J., R. A. Hart, J. T. Kennedy and L. A. Newman: Coupled High Power Waveguide Laser Research. Interim Technical Report under Contract No. F49620-85-C-0106, October 31, 1986.

6. Welch, D. F., et al.: Electron. Lett., Vol. 22, p. 293, 1986.

Section 3.0

7. Bamberger, A., G. Bourdet, B. de Buchere and J. Y Vinet: A High-Frequency Method for Numerical Computation of Modes and Associated Losses of Arbitrary Cross-Section Hollow Waveguides. IEEE Journal of Quantum Electronics, to be published.

8. Jenkins, R. M., and R. W. J. Devereux: Dispersion Phenomena in Hollow Alumina Waveguides. IEEE Journal of Quantum Electronics, Volume QE-21, pp. 1722-1727 (1985). See Figs. 5 and 6.

9. Hall, D. D., E. K. Gorton and R. M. Jenkins: 10 micron Propagation Losses in Hollow Dielectric Waveguides. Journal of Applied Physics, Volume 48, pp. 1212-1216 (1977).

10. Newman, L. A., A. J. Cantor, W. J. Fader, R. A. Hart, J. T. Kennedy and A. J. DeMaria: Coupled High Power Waveguide Laser Research. Final Report on AFOSR Contract F49620-84-C-0062, July 30, 1985.

11. Cantor, A. J., R. A. Hart, J. T. Kennedy and L. A. Newman: Coupled High Power Waveguide Laser Research. Interim Report of AFOSR Contract F49260-85-C-0106, October 31, 1986.

REFERENCES (Cont'd)

Section 3.0

12. Marcatili, E. A. J. and R. A. Schmeltzer: Hollow Metallic and Dielectric Waveguides for Long Distance Optical Transmission and Lasers. The Bell System Technical Journal, pp. 1783-1809 (1964).

13. Laakman, K. D. and W. H. Steier: Waveguides: Characteristic Modes of Hollow Rectangular Dielectric Waveguides. Applied Optics, Volume 15, pp. 1334-1340 (1976).

14. A Simplified Model of Two Coupled Lasers was first presented in two companion papers by M. B. Spencer and W. E. Lamb, Jr.: Laser With a Transmitting Window and Theory of Two Coupled Lasers. Physical Review A, Volume 5, pp. 884-892 and 893-898 (1972).

15. Sargent, M., III, M. O. Scully and W. E. Lamb, Jr.: Laser Physics. Addison-Wesley Publishing Co., Reading (Massachusetts), 1974.

16. This formula is also the standard result for the difference in normal mode frequencies of two coupled oscillators with simple (linear) coupling.

17. See Ref. 10, p. 54.

18. Fader, W. J.: Theory of Two Coupled Lasers. IEEE Journal of Quantum Electronics, Vol. QE-21, pp. 1838-1844 (1985). Also, see Ref. 10, Fig. 31, p. 56 and the related text on p. 54.

19. See Ref. 10, Fig. 30, p. 55.

20. See Ref. 10, Fig. 21, p. 33; and Table 2, pp. 34-35.

21. Butler, J., D. Ackley and D. Botez: Coupled-Mode Analysis of Phase-Locked Injection Laser Arrays. Applied Physics Letters, Vol. 44, p. 293 (1984).

22. Kapon, E., J. Katz and A. Yariv: Supermode Analysis of Phase-Locked Arrays of Semicondcutor Lasers. Optics Letters, Volume 10, pp. 125-127 (1984).

END
DATE
FILM
4-88
DTIC